



HAL
open science

Nitrogen cycle in the Late Archean ferruginous ocean

Vincent Busigny, Oanez Lebeau, Magali Ader, Bryan Krapež, Andrey Bekker

► **To cite this version:**

Vincent Busigny, Oanez Lebeau, Magali Ader, Bryan Krapež, Andrey Bekker. Nitrogen cycle in the Late Archean ferruginous ocean. *Chemical Geology*, 2013, 362, pp.115-130. 10.1016/j.chemgeo.2013.06.023 . hal-03822078

HAL Id: hal-03822078

<https://u-paris.hal.science/hal-03822078v1>

Submitted on 20 Oct 2022

HAL is a multi-disciplinary open access archive for the deposit and dissemination of scientific research documents, whether they are published or not. The documents may come from teaching and research institutions in France or abroad, or from public or private research centers.

L'archive ouverte pluridisciplinaire **HAL**, est destinée au dépôt et à la diffusion de documents scientifiques de niveau recherche, publiés ou non, émanant des établissements d'enseignement et de recherche français ou étrangers, des laboratoires publics ou privés.

1
2
3 **Nitrogen cycle in the Late Archean ferruginous ocean**

4
5
6
7 Vincent Busigny^{1*}, Oanez Lebeau¹, Magali Ader¹, Bryan Krapež², Andrey Bekker³

8
9
10
11
12
13
14 ¹ *Institut de Physique du Globe de Paris, Sorbonne Paris Cité, Univ. Paris Diderot, UMR 7154 CNRS, 1*
15 *rue Jussieu, 75238 Paris, France*

16
17 ² *The Institute for Geoscience Research, Department of Applied Geology, Curtin University, GPO Box*
18 *U1987, Perth WA 6845, Australia*

19
20 ³ *Department of Geological Sciences, University of Manitoba, 125 Dysart Road (Wallace Building),*
21 *Winnipeg, Manitoba, R3T 2N2, Canada*

22
23
24
25
26
27
28 ^{*}Corresponding author. *E-mail address:* busigny@ipgp.fr
29
30
31
32
33
34
35

36 Submitted to Chemical Geology "Dick Holland special volume"
37
38
39
40
41

42 **Abstract**

43
44 The Hamersley Group comprises a Late Archean sedimentary succession, which is
45 thought to record the prelude to the atmospheric oxygenation in the Paleoproterozoic, the so-
46 called Great Oxidation Event (GOE), at ~2.4 Ga. We studied drill-core samples of sedimentary
47 rocks from the upper Mount McRae Shale and Brockman Iron Formation deposited before the
48 GOE at ~2.5 Ga in order to characterize the environments and ecosystems prevailing during their
49 deposition. The rocks from the Mount McRae Shale and Brockman Iron Formation represent,
50 respectively, proximal euxinic conditions and distal ferruginous depositional environments, thus
51 providing an opportunity to examine lateral variability in the open-marine basin. We analyzed the
52 concentration and isotopic composition of carbon in carbonate and organic matter, bulk nitrogen
53 content and its isotopic composition as well as major element concentrations. The $\delta^{13}\text{C}_{\text{carb}}$ values
54 and carbonate content range from -3.2 to -10.7 ‰ and 0.1 to 58 wt%, respectively. Organic
55 carbon content also varies over a large range from 0.05 to 4.6 wt% with a near constant $\delta^{13}\text{C}_{\text{org}}$
56 value of -28.7 ± 0.8 ‰. Negative $\delta^{13}\text{C}_{\text{org}}$ excursions (down to -31 ‰) are generally correlated with
57 high organic matter content. Bulk nitrogen shows highly variable concentration, between 1.3 and
58 785 ppm, and $\delta^{15}\text{N}$ values between 0.4 and 13.4 ‰.

59 The $\delta^{13}\text{C}_{\text{carb}}$ values reflect a diagenetic carbonate origin, with negative values typical for Fe-
60 rich carbonates formed by organic matter mineralization with ferric oxyhydroxides. In contrast,
61 $\delta^{13}\text{C}_{\text{org}}$ and $\delta^{15}\text{N}$ values record primary isotope signatures derived from ancient living organisms.
62 The relatively constant $\delta^{13}\text{C}_{\text{org}}$ values at around -28.7 ‰ are interpreted as reflecting
63 photoautotrophs utilizing a large pool of dissolved inorganic carbon. Inverse stratigraphic co-
64 variation between $\delta^{15}\text{N}$ and $\delta^{13}\text{C}_{\text{carb}}$ values was observed for the Brockman Iron Formation. We

65 propose that N and C biogeochemical cycles were coupled by Fe redox cycling in the water
66 column and in sediments of the Late Archean ocean. Several models for biogeochemical N
67 cycling linked to the redox structure of the water column are considered. Under fully anoxic
68 conditions, the dominant N species available for assimilation by micro-organisms in the photic
69 zone could be ammonium (NH_4^+). Highly positive $\delta^{15}\text{N}$ values would reflect the assimilation of
70 NH_4^+ enriched in ^{15}N by partial oxidation to nitrite, followed by quantitative removal of the
71 produced nitrite by denitrification or anamox processes. Ammonium oxidation could have been
72 driven by (i) O_2 produced locally via oxygenic photosynthesis, or (ii) microbial oxidation utilizing
73 Fe(III)-oxyhydroxides formed in the water column. Under redox-stratified conditions, N
74 assimilated by primary producers could have been in the form of NO_3^- , based on modern and
75 Phanerozoic analogues. The positive $\delta^{15}\text{N}$ values would have resulted in this case from partial
76 denitrification of NO_3^- coupled to anaerobic microbial oxidation of Fe(II) to Fe(III). We conclude
77 that similar positive $\delta^{15}\text{N}$ signatures may record very different N biogeochemical cycles under
78 anoxic, stratified and fully oxic conditions in the ocean. Interpretation of the N isotopes in terms
79 of N biogeochemical cycle thus requires independent constraints on the redox structure of the
80 ocean.

81

82 *Keywords:* nitrogen; carbon; isotopes; Archean ocean; banded iron formation

83

84 **1. Introduction**

85

86 One of the most important changes in Earth's surface history is the oxygenation of the
87 atmosphere-ocean system (Holland, 1984, 2009). The oxygenation imparted major modifications
88 to the geochemical cycles of many redox-sensitive elements, such as C, O, N, S, and base metals,
89 with dramatic implications for the development and evolution of life (Anbar and Knoll, 2002). It
90 is now well established that the first irreversible oxygenation of the atmosphere, the so called
91 Great Oxidation Event (GOE), occurred between 2.4 and 2.3 Ga (Holland, 2002; Bekker et al.,
92 2004; Guo et al. 2009), although transient oxygenation could have occurred earlier. Recent
93 studies of the Mount McRae Shale, Western Australia suggested that atmospheric oxygenation
94 started at 2.5 Ga, based on Mo and Re concentrations and isotopic compositions (Anbar et al.,
95 2007), and C and S isotope values of whole-rock shale samples (Kaufman et al., 2007). Nitrogen
96 isotope (Garvin et al., 2009) and Fe speciation (Reinhard et al., 2009; Raiswell et al., 2011)
97 studies of the same sample set also argued for surface ocean oxygenation at that time. Earlier
98 oxygenation of the surface ocean at ~2.67 Ga was proposed based on N isotope composition of
99 shales from the Campbellrand-Malmani carbonate platform, South Africa (Godfrey and
100 Falkowski, 2009). Besides the question of timing, the secular trend of O₂ accumulation in the
101 atmosphere-ocean system is also highly debated. Two secular trends have been proposed: (1)
102 gradual O₂ increase and accumulation (e.g., Holland, 2006; Murakami et al., 2011), and (2)
103 oscillatory variations in O₂ level in association with the early Paleoproterozoic glacial events and
104 the Lomagundi carbon isotope excursion (Bekker and Kaufman, 2007; Bekker and Holland,
105 2012). The Late Archean may also have been characterized by transient and local low-levels of
106 oxygen, so-called "whiffs" of oxygen (Anbar et al., 2007).

107 Nitrogen isotopes represent a unique tool for exploring the secular evolution of oxygen
108 because (i) N biogeochemistry is mainly controlled by redox reactions and (ii) N is present in all
109 sedimentary rocks, providing a continuous record in different geological settings. In contrast to
110 the Archean, the modern N cycle in the ocean is relatively well understood (see reviews in
111 Brandes et al., 2007; Sigman et al., 2009). The main reservoir of N at the Earth's surface is the
112 atmosphere with a present $\delta^{15}\text{N}$ value of 0 ‰ (N isotope composition is expressed as $\delta^{15}\text{N} =$
113 $[(^{15}\text{N}/^{14}\text{N})_{\text{sample}} / (^{15}\text{N}/^{14}\text{N})_{\text{standard}} - 1] \times 1000$, where the standard is atmospheric N_2). Nitrogen enters the
114 oceanic cycle through atmospheric N_2 fixation by aerobic and anaerobic autotrophs with minor N
115 isotope fractionation (<3 ‰; e.g., Wada et al., 1975; Minagawa and Wada, 1986). After the death
116 of these autotrophic organisms, organic matter mineralization releases N as ammonium (NH_4^+),
117 with very little isotopic fractionation (Prokopenko et al., 2006; Möbius, 2013). In the presence of
118 free O_2 , NH_4^+ is oxidized into nitrate (NO_3^-) during a two-step biological process called
119 nitrification, which is associated with significant N isotope fractionation ~ 16 ‰ (Sigman et al.,
120 2009). This fractionation is rarely fully expressed in modern marine environments since the
121 transformation of NH_4^+ to NO_3^- is generally complete. In O_2 -depleted environments such as
122 oxygen-minimum zones or anoxic sediments, nitrates are partially reduced by denitrification or
123 anammox (i.e., anaerobic ammonium oxidation) into gaseous N_2 or N_2O . During denitrification,
124 ^{14}N is preferentially released relative to ^{15}N , leaving residual marine NO_3^- enriched in the heavy
125 isotope (average marine $\delta^{15}\text{N}_{\text{NO}_3^-} \sim +5$ ‰; e.g., Altabet and François, 1994). The heavy isotope
126 signature of NO_3^- is transferred by assimilation to organisms living in the water column or in the
127 diagenetic realm and then recorded in sedimentary organic matter. Accordingly, assuming a
128 steady-state system, the N isotope composition of organic matter in modern marine environment
129 reflects mainly the relative proportion of N denitrification (in the water column and in sediments)

130 and N fixation. In O₂-free environments such as the Early Archean oceans, the nitrification and
131 thus subsequent denitrification are unlikely, and dissolved N species may have been dominated
132 by NH₄⁺ (Holland, 1984, 2002; Beaumont and Robert, 1999; Papineau et al., 2005). Accordingly,
133 N cycle and isotope composition of Archean ocean and sediments may have been significantly
134 different from those of the modern world (Canfield et al., 2010).

135 Most of the N in the Earth exosphere is contained as N₂ in the atmosphere (presently ~
136 3.98 × 10²¹ g). Based on data from fluid inclusion in cherts (Sano and Pillinger, 1990) and
137 geochemical modeling (Tolstikhin and Marty, 1998), the N isotope composition of the
138 atmosphere is believed to have remained largely constant during the last 3 Ga with δ¹⁵N values of
139 about 0‰. The use of N isotope compositions of Precambrian sedimentary rocks as a tracer of
140 NO₃⁻, and thus O₂, content was proposed in the pioneering work of Beaumont and Robert (1999).
141 In their study, the authors analyzed cherts of various ages and suggested a dramatic change in the
142 N biogeochemical cycle between 3 and 2 Ga. Negative δ¹⁵N values were observed in cherts older
143 than ~2.4 Ga and interpreted as reflecting N₂ fixation or NH₄⁺ assimilation (Beaumont and Robert,
144 1999; Papineau et al., 2005), a result compatible with low NO₃⁻ concentrations (if any) under
145 anoxic conditions in the early Earth oceans. However, this interpretation was questioned since
146 some of these cherts were deposited in hydrothermal settings and may have recorded N isotope
147 signatures of chemoautotrophic organisms specific to these environments (Pinti and Hashizume,
148 2001; Pinti et al., 2001, 2009). If this was the case, their N isotope signature would not reflect
149 phototrophic organisms living in the photic zone of the upper ocean and the N isotope
150 composition of seawater nitrogen compounds. Two recent N-isotope studies of Archean
151 sedimentary sequences from Western Australia and South Africa suggested earlier oxygenation
152 of the Earth's surface ocean starting at 2.5 Ga (Garvin et al., 2009) and 2.67 Ga (Godfrey and

153 Falkowski, 2009), respectively. Both studies identified $\delta^{15}\text{N}$ shifts from near 0 ‰ to positive
154 values, up to 7.5 ‰, and interpreted these trends as evidence for coupled nitrification-
155 denitrification, pathways typical of a surface ocean containing free O_2 . According to their
156 interpretations, denitrification had to be partial so that N isotope fractionation can be expressed.
157 Bulk rock N isotope analyses of ~ 2.72 Ga carbonates from the Tumbiana Formation, Western
158 Australia revealed extreme $\delta^{15}\text{N}$ values up to +50.4 ‰, possibly recording the onset of
159 nitrification coupled to consumption of its products (nitrite and nitrate) via biological
160 denitrification (Thomazo et al., 2011). Such extreme N isotope compositions could only be
161 expressed under oxygen-limited conditions so that partial nitrification would be associated with
162 complete denitrification (Thomazo et al., 2011). High $\delta^{15}\text{N}$ values, up to +20 ‰, were also
163 observed in ~ 2.7 Ga carbonaceous shales from the Western Abitibi Greenstone Belt (Canada) and
164 Penhalonga Formation (Botswana). These values were explained by an Archean ^{15}N -enriched
165 atmosphere resulted from secondary accretion of C1 chondrite-like material (Jia and Kerrich,
166 2004a, 2004b). However, discrete N isotope excursions in time seem more likely than a long-
167 term evolution in composition of the atmosphere since other datasets illustrate very small, if any,
168 N isotope variations in the atmosphere through time (e.g., Sano and Pillinger, 1990; Tolstikhin
169 and Marty, 1998; Marty et al., 2012).

170 Previous studies of N isotopes in Precambrian rocks either (1) focussed on samples of
171 different lithologies and ages from different areas (e.g., Beaumont and Robert, 1999; Papineau et
172 al. 2005, 2009; Pinti et al., 2001, 2009; Jia and Kerrich, 2004b), or (2) analyzed stratigraphic
173 sequences of organic-rich shales (i.e., Garvin et al., 2009; Godfrey and Falkowski, 2009) or
174 carbonates (Thomazo et al., 2011). However, no study has presented so far a stratigraphic dataset
175 for a drill-core section of banded iron formation, which is one of the common Archean

176 sedimentary rocks. In this work, we analyzed the N isotope composition of drill core samples of
177 organic carbon-poor and Fe-rich sediments from the Brockman Iron Formation, Western
178 Australia, one of the best preserved banded iron formations in the world (Trendall and Blockley,
179 1970). The unit contains the products of redox reactions, including Fe oxidation in the water
180 column either by oxygenic or anoxygenic photosynthesis (e.g., Cloud, 1973; Konhauser et al.,
181 2002; Kappler et al., 2005; see also review in Bekker et al., 2010). Systematic N isotope study of
182 banded iron formations has never been performed before since they contain only small amounts
183 of N, requiring high-sensitivity techniques based on static mass-spectrometry. The Brockman
184 Iron Formation was deposited immediately above the Mount McRae Shale, which was
185 extensively studied previously to constrain the redox state of the atmosphere-ocean system
186 (Anbar et al., 2007; Kaufman et al., 2007; Garvin et al., 2009; Reinhard et al., 2009; Raiswell et
187 al., 2011). Accordingly, we build on these previous studies and continue to explore the
188 Hamersley Group in order to constrain environmental changes for the time period between ~2.5
189 and 2.46 Ga. In addition, samples from the Brockman Iron Formation were also selected because
190 they contain stilpnomelane, an Fe-rich mica-like silicate that may have preserved N isotope
191 signatures since NH_4^+ commonly substitutes for K^+ in K-bearing minerals (e.g., Honma and
192 Itihara, 1981; Boyd et al., 2001; Busigny et al., 2003a; Papineau et al., 2005). We found that N
193 concentrations are significantly higher in stilpnomelane-rich shale samples associated with
194 banded iron formation than in previously analyzed banded iron formation and chert samples
195 (Pinti et al., 2001, 2007, 2009). Nitrogen isotope analyses of our samples from the Mount McRae
196 Shale and Brockman Iron Formation were coupled with C isotope analyses of organic matter and
197 carbonates and measurements of major element concentrations. Both elemental and isotopic data
198 are used to separate primary signatures from late diagenetic and metamorphic overprints. Finally,

199 our results are compared to existing data in the literature and previously proposed models in order
200 to further develop and test existing models for the N biogeochemical cycle and redox structure of
201 the early Earth oceans before the GOE.

202

203 **2. Geological setting and sample description**

204

205 The rocks analyzed in our study belong to the Late Archean to early Paleoproterozoic
206 Hamersley Group (Western Australia), and include samples from the Mount McRae Shale and
207 Brockman Iron Formation (Fig. 1). They are composed of laminated and well-preserved
208 sediments that accumulated in relatively deep-water, marine environments below the wave base
209 (Pickard et al., 2004; Kaufman et al., 2007). For the Mount McRae Shale, regional sequence
210 stratigraphic analysis indicates the presence of two depositional cycles; each sequence starts with
211 carbonate and siliciclastic turbidite and breccia and deepens upwards to either semi-pelagic shale
212 or banded iron formation (Krapež et al., 2003). Bulk shale analyses of Re-Os isotopes gave an
213 age of 2501 ± 8 Ma for the Mount McRae Shale (Anbar et al., 2007) consistent with a high-
214 precision SHRIMP ^{207}Pb - ^{206}Pb zircon age of 2504 ± 5 Ma for a tuff layer in the same unit
215 (Rasmussen et al., 2005). The Mount McRae Shale contains large amounts of organic C and
216 pyrite, which are mainly accompanied by quartz, siderite, dolomite, ankerite/ferroan dolomite,
217 chlorite, mica, K-feldspar, albite and minnesotaite (Krapež et al., 2003; Pickard et al., 2004;
218 Raiswell et al., 2011). The upper part of the Mount McRae Shale, the Colonial Chert Member, is
219 transitional to the Brockman Iron Formation (Trendall and Blockley, 1970). The Brockman Iron
220 Formation is composed of four stratigraphic units in ascending order: Dales Gorge, Whaleback
221 Shale, Joffre, and Yandicoogina Shale members (Trendall and Blockley, 1970; Krapež et al.,

222 2003). Depositional ages of \sim 2.48 and 2.46 Ga have been established for the Dales Gorge
223 Member and the Whaleback Shale Member, respectively, based on U-Pb SHRIMP analyses of
224 zircons from tuffaceous layers (Trendall et al., 2004). The Brockman Iron Formation contains
225 alternating hematite-magnetite-chert (BIF) and chert-carbonate-silicate (S) decimeter to meter
226 thick macrobands (Trendall and Blockley, 1970; Krapež et al., 2003; Fig. 1). Macrobands are
227 divided into mesobands (10 to 50 mm in thickness) and laminated microbands (0.2 to 2 mm
228 thick), composed of Fe-oxides, Fe-silicates, Fe-carbonates and chert in variable proportions with
229 minor amounts of pyrite and organic carbon. Banded iron formations of the Brockman
230 Supersequence have long been considered as pure marine chemical precipitates but were recently
231 proposed to reflect episodic density flows (Krapež et al., 2003; Pickard et al., 2004; Rasmussen et
232 al., 2013). Whole-rock major and trace element analyses suggest two dominant sources for BIF
233 and S macrobands, with a major hydrothermal influence and a mafic provenance for BIF and a
234 strong influence of continental and submarine weathering for S macrobands (Krapež et al., 2003;
235 Pickard et al., 2004; Pecoits et al., 2009).

236 In the present work, we selected 31 samples from the Rio Tinto Exploration drill-core
237 WLT-10, collected at 22.73°S and 116.75°E, approximately 100 km WNW from Paraburdoo
238 township close to the south-western margin of the preserved extent of the basin, at depths ranging
239 from 124 to 387 m (Fig. 1; see Table 1 for description of the samples). The samples are
240 uniformly distributed through the uppermost part of the Mount McRae Shale to the unit J3 of the
241 Joffre Member, spanning a depositional period of \sim 40 Ma. The units have experienced only
242 minimal deformation and mild metamorphism (from 100°C to $<$ 300°C; Becker and Clayton,
243 1976; Smith et al., 1982; Kaufman et al., 1990), and carry primary chemical and isotopic
244 signatures. The samples represent different lithologies of the Mount McRae Shale and Brockman

245 Iron Formation, thus allowing global changes in C and N biogeochemical cycles to be
246 distinguished from local variations related to either diagenetic or source-rock effects.

247

248 **3. Analytical techniques**

249

250 For each drill-core sample, uniform layers of 0.5 to 2 cm thick were selected, cut and
251 powdered to <60 μm . Carbon and N isotope analyses together with major element analyses were
252 performed on the same homogeneous powders. For C isotope analysis of carbonates, 3.26 to
253 109.09 mg of rock powder was loaded in a vacutainer tube. The tube was then flushed with
254 helium. Rock powder was treated with 100% phosphoric acid at 80°C for 2 hours and then at
255 130°C for another 2 hours. This treatment secured complete dissolution of carbonate (McCrea,
256 1950). Calcite and dolomite are expected to react at 80°C, while ankerite and siderite react at
257 130°C (Rosenbaum and Sheppard, 1986). Tests on samples subsequently heated to 150°C
258 produced no detectable CO_2 . For each temperature step, C isotope composition of CO_2 was
259 measured using a continuous-flow mass-spectrometer (AP-2003) operated with helium as a
260 carrier gas. The isotopic data are reported in conventional δ units (in per mil) with respect to the
261 V-PDB standard. Analytical error on $\delta^{13}\text{C}$ values is better than ± 0.1 ‰. Carbonate content in
262 samples was estimated from the ion intensity of the CO_2 peak in the mass-spectrometer with a
263 precision better than $\pm 10\%$ (2σ). Two to four replicate analyses of each sample were performed
264 for $\delta^{13}\text{C}_{\text{carb}}$ measurements, but only the average values are presented herein.

265 Total organic C content (TOC) and its C isotope composition were determined on
266 carbonate-free samples. Carbonates from powdered samples were removed using 6N HCl at 80°C
267 for 2 hours. The residue of decarbonation was rinsed with milliQ water several times until it

268 reached neutral pH, centrifuged and dried for 2 days at 50°C. Mass balance was used to estimate
269 the amount of removed carbonate. Aliquots of dried decarbonated samples (50 to 100 mg for the
270 Brockman Iron Formation samples and <10mg for the Mount McRae Shale samples) were then
271 loaded into quartz tubes together with CuO wires, sealed under vacuum and combusted at 950°C
272 for 6 hr (Duma combustion; cf., Bekker et al., 2001, Ader et al., 2006, 2009; Thomazo et al.,
273 2009a; Sansjofre et al., 2011). The produced CO₂ was purified on a vacuum line and quantified
274 manometrically; TOC content reproducibility was better than ±0.3 wt%. Carbon isotope
275 composition of the purified CO₂ was then measured on a Delta^{plus}XP mass-spectrometer with a
276 precision better than ±0.1 ‰. Results are reported using the δ¹³C notation in per mil relative to V-
277 PDB.

278 The procedure used for measurement of nitrogen content and its isotopic composition in
279 rocks has been thoroughly described in previously published papers (Busigny et al., 2005; Ader
280 et al., 2006) and is only summarized herein. Nitrogen was extracted from samples by combustion
281 in quartz tubes sealed under vacuum. Before sample combustion, the powders were degassed
282 under vacuum at 300°C for 12hrs. This degassing temperature is different from that previously
283 used (450°C; Busigny et al., 2005; Ader et al., 2006) and was preferred for two reasons: (1) the
284 Mount McRae Shale and Brockman Iron Formation have experienced a maximum burial
285 temperature of 300°C (Smith et al., 1982; Kaufman et al., 1990), and (2) stilpnomelane, a
286 potential N-bearing mineral phase, starts to break down at 450°C (Miyano and Klein, 1989).
287 Nitrogen generated by combustion was then separated from other volatiles (mainly H₂O and CO₂)
288 using purified Cu, CuO, and CaO (Kendall and Grim, 1990). It was quantified as dinitrogen (N₂)
289 with a capacitance manometer on ultra-high vacuum line and its isotope analysis was performed
290 on a triple-collector static vacuum mass-spectrometer, allowing measurement of nanomole

291 quantities of N₂. Nitrogen isotope composition is expressed in the δ¹⁵N notation in per mil relative
292 to atmospheric N₂. The quantity of N contributed by the analytical blank is low (0.65 ± 0.30 nmol
293 N₂) and its isotope composition is -3.7 ± 2.7 ‰ (2σ). The precisions for sample nitrogen content
294 and its isotope composition are better than 8% and 0.5 ‰, respectively.

295 Whole-rock concentrations of major elements were measured using ICP-AES at the
296 Service d'Analyse des Roches et des Minéraux (SARM) of the Centre de Recherches
297 Petrographiques et Géochimiques (CRPG) of Vandoeuvre, France. Analytical precision for major
298 element concentrations is available at <http://helium.crpq.cnrs-nancy.fr/SARM/pages/roches.html>
299 and typically better than 10%.

300

301 **4. Results**

302

303 *4.1. Major element concentrations linked to petrology*

304

305 Correlations observed between some major elements (Fig. 2) supports the identification of
306 lithologies established during drill-core sampling and petrographic study. This shows a diversity
307 of chemical compositions between several mineralogical end-members. Positive correlation
308 among Al₂O₃, SiO₂, and K₂O (Fig. 2a and 2b) indicates that these elements are contained in the
309 same phases, mostly stilpnomelane, but also mica and K-feldspar. Only one sample (DGM307-6)
310 shows strong enrichment in SiO₂ (73 wt%) with no associated enrichment in Al₂O₃ (0.2 wt%).
311 This sample is identified as a chert based on petrography. For all samples, an inverse correlation
312 between Fe₂O₃ and SiO₂ (Fig. 2c) indicates that Fe-silicates do not represent one of the dominant
313 Fe-bearing phases, in contrast to Fe-oxides (hematite and magnetite) and Fe-carbonates (siderite

314 and ankerite). It should be noted that our samples from the Mount McRae Shale differ from those
315 of the Brockman Iron Formation in containing dolomite as a dominant carbonate phase while Fe-
316 rich carbonates were not found by electron microprobe analysis. In contrast to the relationship
317 between Al_2O_3 and K_2O , the best-fit line for Al_2O_3 and SiO_2 does not pass through the origin on the
318 graph (Fig. 2a). Indeed, SiO_2 is at 10 to 20 wt%, when Al_2O_3 concentration is close to 0 wt%. This
319 observation, coupled with petrography, indicates that most of our samples contain quartz (chert).
320 Samples from the Brockman Iron Formation are strongly enriched in Fe with Fe_{Total} (expressed as
321 Fe_2O_3) concentrations ranging from 6.7 to 78.2 wt% and averaging 33.8 ± 15.5 wt% (n=26). This
322 differs significantly from the Mount McRae Shale samples, which have Fe_{Total} concentrations
323 between 2.3 and 6.2 wt% (average is 3.8 ± 1.6 wt%, n=5). This contrast is also reflected in Fe/Ti
324 molar ratios (Fig. 3). Fe-enrichment of the Brockman Iron Formation likely reflects
325 contemporaneous anoxic and ferruginous conditions in the deep ocean (cf., Bekker et al., 2010),
326 while the depositional environment of some portions of the Mount McRae Shale has been
327 interpreted as anoxic and sulfidic (e.g., Reinhard et al., 2009; Raiswell et al., 2011).

328 To conclude, samples from the Brockman Iron Formation are mostly composed of
329 potassium- and aluminum-rich silicates, Fe-oxides, quartz and carbonates in variable proportions.
330 According to mineralogy and major element composition, our samples were divided into five
331 rock types: organic-rich shale from the Mount McRae Shale, and stilpnomelane-rich mudrock,
332 banded iron formation and chert from the overlying Brockman Iron Formation. Stilpnomelane-
333 rich mudrocks were furthermore subdivided based on their carbonate content into carbonate-rich
334 (>10 wt%) and carbonate-poor (<10 wt%) varieties.

335

336 4.2. Carbon content and its isotope composition

337
338 Carbonates contained in samples from the Mount McRae Shale were completely extracted
339 at temperature below 80°C and no signal was detected at 130°C, confirming that they contain no
340 siderite. About half of our samples from the Brockman Iron Formation were fully decarbonated at
341 80°C, while the other half still contained carbonate, which was extracted at 130°C. This clearly
342 points to the presence of siderite in half of these samples (Rosenbaum and Sheppard, 1986).
343 However, for both extraction temperatures (80°C and 130°C), $\delta^{13}\text{C}_{\text{carb}}$ values are nearly identical
344 within $\pm 0.5\text{‰}$. Thus, only bulk carbonate content and average $\delta^{13}\text{C}_{\text{carb}}$ values will be considered in
345 the following discussion. For the Brockman Iron Formation, the bulk carbonate content varies
346 greatly from less than 0.1 up to 83 wt%. The range of carbonate content in the Mount McRae
347 Shale from 8 to 57 wt% is smaller but still significant. The $\delta^{13}\text{C}_{\text{carb}}$ values measured in samples
348 from the Brockman Iron Formation (-10.7 to -5.1 ‰) are lower than those measured in samples
349 from the Mount McRae Shale (-5.6 to -3.2 ‰). The chemostratigraphic profile of C isotope
350 composition in carbonates shows significant variations, with intervals of increasing and
351 decreasing $\delta^{13}\text{C}_{\text{carb}}$ values (Fig. 4).

352 Depth profiles of C_{org} content and $\delta^{13}\text{C}_{\text{org}}$ values within the core are shown on Fig. 4. Data
353 for the Mount McRae Shale from Garvin et al. (2009) are also plotted for comparison. A strong
354 contrast is noticeable between samples from the Mount McRae Shale and Brockman Iron
355 Formation. The Mount McRae Shale is enriched in organic C with concentrations ranging from
356 1.7 to 16.1 wt% (average = 5.7 ± 3.8 wt%, 1σ), while samples from the Brockman Iron
357 Formation contain between 0.05 and 1.9 wt% of C_{org} (average = 0.7 ± 0.5 wt%, 1σ). This contrast
358 is even more pronounced in C_{org} isotope values, which roughly show a bimodal distribution with

359 the sharp transition from the Mount McRae Shale to the Brockman Iron Formation (Fig. 4). The
360 Mount McRae Shale has markedly negative $\delta^{13}\text{C}_{\text{org}}$ values, averaging $-37.6 \pm 2.8 \text{ ‰}$ (1σ), in
361 contrast to the Brockman Iron Formation with a mean $\delta^{13}\text{C}_{\text{org}}$ value of $-28.7 \pm 0.8 \text{ ‰}$ (1σ). The
362 heaviest C isotope composition (-26.4 ‰) is found in the chert DGM307-6 of the Brockman Iron
363 Formation, and corresponds to the lowest C_{org} content (0.05 wt%). The organic carbon content of
364 our complete sample set shows an inverse trend with Fe/Ti molar ratio (Fig. 3a), indicating that
365 Fe enrichment is associated with organic C depletion. Organic carbon contents also roughly
366 correlate with $\delta^{13}\text{C}_{\text{carb}}$ values with the most negative $\delta^{13}\text{C}_{\text{carb}}$ values corresponding to the lowest C_{org}
367 contents (Fig. 5).

368

369 *4.3. Nitrogen content and isotope composition*

370

371 Depth profiles of N content and $\delta^{15}\text{N}$ values within the drill-core are shown in Fig. 4.
372 Nitrogen content shows a similar stratigraphic pattern to that of C_{org} content (Fig. 4). This is also
373 illustrated by the positive correlation between these parameters (Fig. 6a). Samples from the
374 Mount McRae Shale are enriched in N with concentrations ranging between 385 and 786 ppm
375 (average = $495 \pm 169 \text{ ppm}$, 1σ). In contrast, samples from the Brockman Iron Formation are
376 characterized by significantly lower N contents from 1.3 to 186 ppm (average = $55 \pm 50 \text{ ppm}$,
377 1σ). Like organic C, N content decreases with increasing Fe/Ti molar ratio, indicating that Fe
378 enrichment is associated with low N concentrations (Fig. 3b). $\text{C}_{\text{org}}/\text{N}$ molar ratios for the Mount
379 McRae Shale vary from 45 to 127 (average = 70 ± 35 , 1σ). On the average, they are lower
380 compared to samples from the Brockman Iron Formation (mostly between 19 and 895, the
381 average is 242 ± 200 , 1σ). Only one sample of the Brockman Iron Formation shows an

382 exceptionally high C_{org}/N ratio of 2251 (sample DGM288-2, Table 3). This high value is
383 geologically relevant and is not an analytical artefact from incomplete carbonate dissolution,
384 since this sample shows a $\delta^{13}C_{org}$ value of -29‰ , indistinguishable from other samples (even minor
385 carbonate contamination would significantly increase the measured $\delta^{13}C$ value). The depth profile
386 of N isotope composition shows large variations in $\delta^{15}N$ values. These variations are independent
387 of rock lithology, with N isotope values of organic-rich shale, carbonate-rich and carbonate-poor
388 stilpnomelane mudrock, banded iron formation and chert fitting to the broad trend (Fig. 4). The
389 $\delta^{15}N$ values range from 4.4 to 5.7 ‰ for the Mount McRae Shale (average = $4.9 \pm 0.6 \text{‰}$, 1σ) and
390 from 0.4 to 13.4 ‰ for the Brockman Iron Formation (average = $7.5 \pm 2.7 \text{‰}$, 1σ). Pinti et al.
391 (2001) analyzed one banded iron formation sample, containing magnetite, quartz and chlorite,
392 from the Dales Gorge Member of the Brockman Iron Formation and found N content and $\delta^{15}N$
393 value of 1.9 ppm and 11.5 ‰, respectively, within the range of the present data. In our sample
394 set, N isotope values do not show any correlation with N content, C_{org}/N ratios (Fig. 7), or $\delta^{13}C_{org}$
395 values. The chemostratigraphic profile shows a generally inverse correlation between $\delta^{15}N$ and
396 $\delta^{13}C_{carb}$ values (Fig. 4). However, a plot of $\delta^{15}N$ versus $\delta^{13}C_{carb}$ values does not clearly show any
397 correlation between these two parameters ($r^2 = 0.31$; Fig. 7c), suggesting that they are only
398 indirectly linked to each other.

399

400 **5. Discussion**

401

402 Before any discussion about paleoenvironmental implications of our results can take
403 place, it is important to establish whether measured C and N contents and isotope compositions

404 preserved a primary signature, i.e., one generated in the water column, or one that has been
405 produced by later processes such as diagenesis or low-grade metamorphism.

406

407 *5.1. Evidence for primary C isotope composition of organic matter*

408

409 In sedimentary rocks, large variations in organic carbon content may reflect changes in (1)
410 primary productivity (i.e., production of microbial photoautotrophic biomass), (2) degree of
411 recycling of organic matter in the water column and in sediments during diagenesis, (3) extent of
412 thermal maturation of carbonaceous materials associated with sediment burial, and (4)
413 sedimentation rate resulting in organic matter dilution or concentration. These controls are further
414 explored below. Thermal maturation of organic molecules releases carbon (in the form of
415 hydrocarbons; e.g., CH₄), preferentially enriched in ¹³C, and may lead to a significant decrease in
416 C_{org} content associated with an increase in δ¹³C values of the residual organic matter (Hayes et al.,
417 1983). This isotope effect is small for metamorphic grades lower than the upper greenschist
418 facies (typically <2‰) and can thus be neglected in the present case since the Mount McRae
419 Shale and Brockman Iron Formation have experienced metamorphic temperatures <300°C
420 (Becker and Clayton, 1976; Smith et al., 1982; Kaufman et al., 1990, 2007). An important
421 observation for our samples is the relationship between C_{org} content and Fe/Ti molar ratios (Fig.
422 3a). Because Ti is immobile in any kind of aqueous fluid, the sedimentary flux of Ti mostly
423 reflects detrital contributions. If we assume a constant Fe/Ti molar ratio for the detrital source,
424 then an increase in Fe/Ti molar ratio in the sedimentary rocks will track an increase in the flux of
425 authigenic Fe (e.g., Dauphas et al., 2007a, 2007b). Accordingly, Fig. 3a shows that C_{org} content is
426 inversely proportional to the flux of authigenic Fe to the sediment. Previous studies of Archean

427 sedimentary rocks also identified an inverse relationship between C_{org} and Fe contents and
428 proposed that it reflects the role of Fe-oxyhydroxides in mineralization of organic matter (e.g.,
429 Walker, 1984; Beukes et al., 1990; Kaufman et al., 1990; Bekker et al., 2010). In this scenario,
430 ferric iron precipitate acts as an electron acceptor during early diagenesis for organic matter
431 oxidation. This explanation is supported by the inverse correlation between C_{org} contents and Fe/Ti
432 molar ratios (Fig. 3a), implying that C_{org} content was likely influenced to variable degree by
433 organic-matter mineralization. An important question is whether this mineralization process
434 imparted any modification to the C isotope composition of organic matter. If mineralization was
435 associated with C isotope fractionation, then $\delta^{13}\text{C}$ values should show some correlation with C_{org}
436 contents. This is not the case and in contrast to large variations in C_{org} content, $\delta^{13}\text{C}_{\text{org}}$ values of the
437 Brockman Iron Formation show only moderate variability and can be regarded as constant at
438 about $-28.7 \pm 0.8 \text{ ‰}$ (1σ). The possibility of a modern contamination — related to sampling or
439 analytical procedures — with a source having a homogeneous $\delta^{13}\text{C}$ value seems unlikely, since C_{org}
440 contents would be similar in all of the samples and would not show a stratigraphic trend (Fig. 4).
441 The remarkable isotopic constancy for the whole range of lithologies suggests that modification
442 of the $\delta^{13}\text{C}_{\text{org}}$ values was minor after sediment deposition. We therefore argue that the C isotope
443 composition of organic matter measured in our study represents the primary organic carbon
444 signature of the microorganisms thriving in the water column. The constancy of $\delta^{13}\text{C}_{\text{org}}$ values also
445 indicates that C was assimilated from a homogeneous pool of dissolved inorganic carbon, with
446 constant (or near constant) C isotope composition. The few samples of the Brockman Iron
447 Formation significantly diverging from the mean $\delta^{13}\text{C}_{\text{org}}$ value may have organic matter generated
448 via at least two different metabolic pathways imposing different carbon isotope fractionations.
449 The chert sample (DGM307-6) has a particularly low C_{org} content and high $\delta^{13}\text{C}_{\text{org}}$ value of 0.05

450 wt% and -26.4 ‰, respectively, and could have been affected by intense loss of organic matter
451 during diagenesis. Three samples in our study have $\delta^{13}\text{C}_{\text{org}}$ values significantly lower than the
452 average $\delta^{13}\text{C}_{\text{org}}$ value of -28.7 ± 0.8 ‰ (samples DGM287, DGM288-1, and MR387). These lower
453 $\delta^{13}\text{C}_{\text{org}}$ values are associated with high C_{org} contents ($> 1\text{wt}\%$; see Table 2). On the stratigraphic
454 profile (Fig. 4), they fit well with $\delta^{13}\text{C}_{\text{org}}$ values previously measured for the Mount McRae Shale,
455 having even more negative values down-section (as low as -41.6 ‰; data from Kaufman et al.,
456 2007 and Garvin et al., 2009). These negative $\delta^{13}\text{C}$ values have been related to the activity of
457 methanotrophic organisms (Kaufman et al., 2007). Accordingly, our samples with markedly
458 negative $\delta^{13}\text{C}_{\text{org}}$ values may also contain some organic matter derived from methanotrophic
459 microbes.

460

461 *5.2. Carbonate precipitation during diagenesis*

462

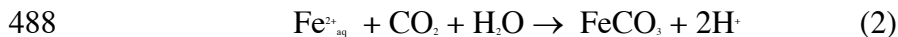
463 Sedimentary carbonates record the isotopic composition of dissolved inorganic carbon
464 (DIC) pool from which they precipitated with a positive offset of ~ 1 ‰ due to thermodynamic
465 isotope equilibrium (e.g., Morse and Mackenzie, 1990; for siderite see Zhang et al., 2001, and
466 references therein). Their $\delta^{13}\text{C}_{\text{carb}}$ and $\delta^{13}\text{C}_{\text{org}}$ values can be used to deduce the isotope fractionation
467 associated with carbon assimilation ($\Delta^{13}\text{C} = \delta^{13}\text{C}_{\text{carb}} - \delta^{13}\text{C}_{\text{org}}$), which is a proxy for metabolic
468 processes (e.g., Hayes et al., 1999; Bekker et al., 2001, 2008; Thomazo et al., 2009b; Bekker and
469 Kaufman, 2007; Sansjofre et al., 2011).

470 In our samples of the Brockman Iron Formation, $\delta^{13}\text{C}_{\text{org}}$ values show little variation over
471 the stratigraphic profile (Fig. 4). It implies that living organisms thrived in a homogeneous pool
472 of dissolved inorganic carbon with a constant $\delta^{13}\text{C}$ value. In contrast, $\delta^{13}\text{C}_{\text{carb}}$ values show large

473 variability among the samples, implying that not all carbonates precipitated from the same pool
474 of dissolved inorganic carbon as that utilized by organic matter. A portion (if not all) of the
475 carbonates could have precipitated from either (1) a deep layer of the stratified water column
476 (Beukes et al., 1990), or (2) sediment porewaters during diagenesis (Walker, 1984). Petrographic
477 and geochemical data supports the second scenario. Petrographic observations show that many
478 carbonates in the Brockman Iron Formation cement matrix minerals, indicating that they formed
479 after sedimentary components were deposited. Another argument derives from the rough
480 correlation between C_{org} contents and $\delta^{13}C_{carb}$ values (Fig. 5). Low C_{org} content might reflect
481 mineralization of organic matter during sediment diagenesis (see discussion in section 5.1).
482 Correlation between C_{org} contents and $\delta^{13}C_{carb}$ values then may indicate that the more organic matter
483 was mineralized, the more negative $\delta^{13}C$ values were imprinted on carbonates. This can be
484 explained by a two-stage process: (1) organic matter degradation via ferric-oxyhydroxide
485 reduction, which increases ferrous iron and CO_2 content in solution as in the following reaction:



487 (2) precipitation of iron-rich carbonates from sediment pore-waters such as:



489 Based on this model, we could expect a correlation between $\delta^{13}C_{carb}$ value and the amount or
490 proportion of siderite (or other Fe-carbonate) in our samples, as represented by the carbonate
491 fraction extracted at the temperature of $\sim 130^\circ C$ (Table 3). Such a correlation is not observed
492 possibly because many carbonates are not pure siderites but mixed Fe-Ca-Mg carbonates, which
493 may have formed during diagenesis or later by carbonate recrystallization during sediment burial.
494 In any case, it does not contradict the possibility of diagenetic carbonate formation during organic
495 matter degradation via ferric-oxyhydroxide reduction, but it suggests that diagenetic Fe-

496 carbonates are not exclusively siderites. A similar mechanism for carbonate precipitation was
497 also inferred based on $\delta^{13}\text{C}$ data obtained for carbonates and organic matter from the Late Archean
498 Transvaal Supergroup in South Africa (Fischer et al., 2009). It was also proposed based on
499 coupling of Fe and C isotope values in the Late Archean carbonate-bearing iron formations
500 (Heimann et al., 2010; Craddock and Dauphas, 2011), suggesting that this process could have
501 been common during the Late Archean.

502

503 *5.3. Preservation of N isotope signature in organic matter*

504

505 Like for carbon, it is important to determine if N isotope composition reflects a signature
506 of organisms living in the water column or was affected by late modifications related to post-
507 depositional processes. This is crucial since late-stage hydrothermal processes have been invoked
508 for iron formation in some localities within the Hamersley Province (Webb et al., 2003).
509 Correlation between N and C_{org} contents suggests that N originated from organic matter (Fig. 6a).
510 Since organic C is likely predominantly derived from primary producers, the same origin might
511 equally apply to N. Samples from the Brockman Iron Formation have C_{org}/N molar ratios
512 averaging 242 ± 200 (1σ), which is similar to the average C_{org}/N molar ratio of the previously
513 measured Archean cherts from various localities including Western Australia, South Africa and
514 Northern America (200.7 ± 137 , 1σ , $n=59$; Beaumont and Robert, 1999; Ueno et al., 2004, Pinti
515 et al., 2007, 2009). Similarly to carbon content, nitrogen content is negatively correlated with
516 Fe/Ti molar ratio, suggesting that N was also removed from the sediment by organic matter
517 mineralization (Fig. 3b; see discussion on organic carbon content in section 5.1). The lowest N

518 content corresponds to the chert sample DGM307-6 that contains ~1.3 ppm N, and is similar to
519 some other Archean chert samples in nitrogen content (Pinti et al., 2001, 2007, 2009).

520 Nitrogen content shows a broad positive correlation with K_2O content (Fig. 6b). This
521 suggests that part of the nitrogen released to sediment porewaters during organic matter
522 mineralization, was substituted in the form of NH_4^+ for K^+ in K-bearing minerals, because of their
523 similar charge and ionic radius (Honma and Itihara, 1981; Busigny et al., 2003a; Rouchon et al.,
524 2005). In other words, C and N were likely supplied from the same organic material but
525 diagenetic evolution induced a loss of N from organic matter with partial incorporation as NH_4^+
526 into K-minerals. Since N is preferentially released from organic matter during diagenesis and
527 metamorphism with respect to C, C/N ratio can be used as a proxy to evaluate the effect of these
528 processes on N content and its isotopic composition (Ader et al., 2006; Boudou et al., 2008).
529 Decrease in C/N ratio with increasing K_2O content confirms that part of the N released from
530 organic matter was fixed as NH_4^+ in K-silicates and was then protected from diagenesis and early
531 metamorphism (Fig. 6c). One banded iron formation sample (DGM364), plotting away from the
532 general K_2O -N trend, represents particularly high N content with respect to its K_2O and C_{org}
533 contents (83.9 ppm N, 0.12 wt% K_2O , and 0.59 wt% C_{org} ; Fig. 6a and b). This sample shows the
534 highest Fe_{total} concentration, having 78.16 wt% Fe_2O_3 . It might indicate that N was predominantly
535 bound with Fe oxides, as was earlier suggested by Pinti et al. (2007). Since N isotopes could be
536 fractionated during organic matter degradation, it is important to evaluate whether N isotope
537 signature of our samples records paleo-ecosystem and paleo-environmental (e.g., redox)
538 conditions. Organic matter degradation occurs (1) in the water column and in the sediment during
539 early diagenesis, and (2) during thermal maturation associated with burial diagenesis and
540 metamorphism. In oxic environments, early diagenesis may impart a shift in $\delta^{15}N_{org}$ values

541 towards more positive values with a magnitude reaching ~ 3 ‰ (e.g., Altabet and Francois, 1994;
542 Lehmann et al., 2002; Gaye et al., 2009; Möbius et al., 2010). In contrast, organic matter
543 degradation under anoxic and suboxic conditions either preserves original nitrogen isotope values
544 or slightly lowers $\delta^{15}\text{N}_{\text{org}}$ values with a shift smaller than 1 ‰ (e.g., Lehmann et al., 2002; Thunell
545 et al., 2004; Möbius et al., 2010). In the case of the Brockman Iron Formation, the deep waters of
546 the basin were clearly anoxic as indicated by (i) the particularly high Fe content in the sediments
547 requiring high dissolved Fe(II) concentrations, and (ii) REE patterns lacking a negative Ce
548 anomaly and with a pronounced positive Eu anomaly reflecting a source of reduced, high-
549 temperature fluids similar to modern, mid-ocean ridge hydrothermal systems (e.g., Klein and
550 Beukes, 1989; Alibert and McCulloch, 1993; Beukes and Gutzmer, 2008; Planavsky et al., 2010).
551 Accordingly, $\delta^{15}\text{N}$ values of our samples were probably not or only slightly modified during early
552 diagenesis in this anoxic depositional setting. Effect of thermal maturation associated with burial
553 diagenesis and metamorphism on N isotope composition can be tested using tracers such as N
554 concentration and C/N ratio. Studies on coal with variable maturity showed that as metamorphic
555 grade increases, organic N content decreases and $C_{\text{org}}/N_{\text{org}}$ ratio increases, while $\delta^{15}\text{N}$ values remain
556 largely unaffected (Ader et al., 1998, 2006; Boudou et al., 2008). However, if N present in form
557 of NH_4^+ in silicate minerals is lost during metamorphism then the residual $\delta^{15}\text{N}$ values could be
558 increased by up to a few per mil (Bebout and Fogel, 1992; Mingram and Braüer, 2001; Bebout et
559 al., 1999; Busigny et al., 2003b; Jia, 2006). In our sample set, N contents and C/N ratios do not
560 show any significant correlation with $\delta^{15}\text{N}$ values (Fig. 7a and b), thus suggesting that $\delta^{15}\text{N}$ values
561 are not controlled by N loss during sediment burial and metamorphism. In support of this
562 statement, the stratigraphic trend of $\delta^{15}\text{N}$ values within the drill-core shows smooth alternating
563 rises and falls of $\delta^{15}\text{N}$ values suggesting either a secular or local control over N isotope variations

564 (Fig. 4) rather than that imposed by post-depositional modification. We conclude that the $\delta^{15}\text{N}$ and
565 $\delta^{13}\text{C}_{\text{org}}$ values of our samples from the Brockman Iron Formation and Mount McRae Shale mostly
566 reflect primary organic matter composition.

567

568 *5.4. Implications for ancient N biogeochemical cycle*

569

570 In this section, the elemental concentrations and isotopic variations of N-C_{org}-C_{carb}-Fe in the
571 Mount McRae Shale and Brockman Iron Formation are integrated to explore several models of N
572 biogeochemical cycle in the Late Archean ocean. For all herein discussed models, we assume the
573 following lateral distribution of sedimentary facies from proximal to distal, deep-sea
574 environments (cf., Beukes et al., 1990; Bekker et al., 2010): (1) organic matter-rich, sulfidic
575 shales deposited under euxinic conditions, (2) iron-rich shales and carbonates, and (3) banded
576 iron formations and chert in deeper settings (Fig. 8). Nutrients sustaining organic productivity
577 were predominantly supplied from the continents or by coastal upwelling currents, resulting in
578 higher organic productivity in proximal facies. Part of the Mount McRae Shale was deposited
579 under euxinic conditions (Reinhard et al., 2009; Raiswell et al., 2011), where accumulation of
580 free H₂S in the water column in excess of dissolved Fe²⁺ might have resulted from either riverine
581 delivery of SO₄²⁻ produced by oxidative continental weathering or atmospheric supply of sulphate
582 aerosols generated in the anoxic atmosphere by UV photolysis (Bekker et al., 2010), combined
583 with bacterial SO₄²⁻ reduction associated with the remineralisation of organic matter. The Mount
584 McRae Shale high organic productivity, reflected in its elevated C_{org} concentrations, is associated
585 with markedly negative $\delta^{13}\text{C}_{\text{org}}$ values (Figure 4) suggesting high methanotrophic contributions to
586 the organic matter (Kaufman et al., 2007). Methanotrophs have two specific requirements. First, a

587 flux of methane, likely derived from preferential organic matter mineralization by methanogens
588 under low oxygen conditions. For the Mount McRae Shale, the low Fe/Ti ratios (Figure 3)
589 indicate that ferric iron availability was limited, therefore favouring methanogenesis as the
590 dominant degradation pathway in the deeper part of the water column and in the sediment
591 porewaters. Second, methanotrophic organisms require oxidant availability so that methane is
592 oxidized via either anaerobic, with, for example, sulphate as an electron acceptor, or aerobic
593 oxidation (Hayes et al., 1983; Thomazo et al., 2009a). The upper part of the water column in the
594 Mount McRae Shale depositional environment therefore should have contained either dissolved
595 oxygen or another oxidant such as sulphate, nitrate, or Fe- and Mn-oxyhydroxides. In contrast to
596 the Mount McRae Shale, the biomass in the Brockman Iron Formation depositional setting was
597 probably dominated by photosynthetic organisms, either oxygenic or anoxygenic.
598 Chemoautotrophic organisms living in hydrothermal systems were also proposed as the main
599 source of organic matter for Archean cherts (Pinti and Hashizume, 2001; Pinti et al., 2001, 2009).
600 This source of organic carbon and nitrogen seems unlikely for our samples from the Brockman
601 Iron Formation both because of their geological setting (no evidence for active hydrothermal
602 systems at the depositional site of this unit) and their $\delta^{15}\text{N}$ and $\delta^{13}\text{C}$ values, which are not as
603 negative as those typical of chemoautotrophs (e.g., $\delta^{15}\text{N}$ values as low as -5 ‰ and $\delta^{13}\text{C}$ values
604 lower than -40 ‰). The $\delta^{13}\text{C}$ values of our samples (-28.7 ± 0.8 ‰; Fig. 4) are compatible with
605 primary producers living in the photic zone of the water column. The ferric iron flux to the
606 depositional site of the Brockman Iron Formation was obviously higher than that to the
607 depositional site of the Mount McRae Shale, as illustrated by their Fe/Ti ratios (Fig. 3). This
608 suggests that anaerobic respiration using iron oxyhydroxide reduction may have been the
609 dominant degradation pathway for organic matter, which is energetically more favourable than

610 methanogenesis. Iron oxyhydroxide reduction would have increased dissolved Fe(II) and DIC
611 concentrations in porewaters, likely inducing Fe-rich carbonate precipitation with low $\delta^{13}\text{C}_{\text{carb}}$
612 values (see discussion in section 5.2). The chemostratigraphic profiles presented in Figure 4 show
613 roughly inverse trends for $\delta^{15}\text{N}$ and $\delta^{13}\text{C}_{\text{carb}}$ values in the Brockman Iron Formation. Since $\delta^{13}\text{C}_{\text{carb}}$
614 values likely reflect a diagenetic origin of Fe-rich carbonates, $\delta^{15}\text{N}$ variations might be also
615 interpreted as resulting from organic matter degradation. However, the discussion presented
616 above in section 5.3 as well as a weak direct correlation between $\delta^{15}\text{N}$ and $\delta^{13}\text{C}_{\text{carb}}$ values (Fig. 7c)
617 suggest that $\delta^{15}\text{N}$ values more likely represent the primary signature of organic matter in the water
618 column, i.e. the N isotope composition of photosynthetic organisms. It seems likely therefore that
619 N and C_{carb} isotope compositions were linked by indirect processes.

620 According to previous studies, two possible scenarios can be considered for the redox
621 structure in the water column of the Late Archean oceans. In the first case, the water column is
622 stratified with a thin oxygenated (oxic or disoxic) upper layer overlying an anoxic and
623 ferruginous lower layer (e.g., Beukes and Gutzmer, 2008). This scenario is traditionally invoked
624 to explain deposition of banded iron formations, where upwelling dissolved Fe(II) is oxidized
625 with O_2 produced through photosynthetic activity of cyanobacteria (Cloud, 1973; Klein and
626 Beukes, 1989). The second scenario infers a fully anoxic water column (e.g., Planavsky et al.,
627 2010) with banded iron formation deposition controlled by one or several of the following
628 processes: metabolic Fe(II) oxidation, UV photooxidation, or quantitative consumption of
629 produced O_2 (e.g., Bekker et al., 2010). In both models for iron formation deposition, nitrogen
630 from the atmosphere was initially introduced into the ocean by N_2 -fixing organisms, such as
631 cyanobacteria, under either aerobic or anaerobic conditions. Nitrogen assimilated by these
632 organisms is not strongly fractionated in the modern ocean ($\delta^{15}\text{N} \approx 0 \text{‰}$; e.g., Minagawa and

633 Wada, 1986), but can have negative values (as low as -3 ‰) when N₂-fixing organisms are grown
634 in Fe-enriched media (Zerkle et al., 2008). After death of N₂-fixing bacteria, they would sink
635 through the water column and would be incorporated into sediments resulting in δ¹⁵N values of
636 sedimentary organic matter around 0 ‰. Nitrogen from their nucleic and amino acids can be
637 partially released as ammonium (NH₄⁺) by mineralization in the water column or in sediments.
638 Further processing of NH₄⁺ will depend on local redox conditions. The positive δ¹⁵N values of the
639 Mount McRae Shale and Brockman Iron Formation indicate that N₂-fixing organisms were not
640 the only source of organic matter to the sediment. Positive δ¹⁵N values of this magnitude in
641 Precambrian rocks can be caused by three different pathways: (1) partial assimilation of
642 ammonium (Papineau et al., 2009), (2) partial nitrification of ammonium, followed by complete
643 denitrification of the produced nitrite (Thomazo et al., 2011), and (3) quantitative oxidation of
644 ammonium to nitrate, followed by partial denitrification in the water column (Godfrey and
645 Falkowski, 2009; Garvin et al., 2009). The cases 1 and 2 require global anoxic conditions for
646 ammonium to be stable in the water column under open-marine conditions. In contrast, case 3
647 requires an oxic photic zone for nitrate stability, with limited denitrification under suboxic
648 conditions, similar to an oxygen minimum zone of the modern ocean. For all 3 cases, the rises
649 and falls of δ¹⁵N values in the Mount McRae Shale and Brockman Iron Formation would be
650 produced by variations in the relative proportion of N₂-fixation and ¹⁵N-enriched NO₃⁻ or NH₄⁺
651 assimilation. The Mount McRae Shale has lower δ¹⁵N values (the average is 3.8 ± 1.7 ‰, n = 82;
652 Garvin et al., 2009) than the Brockman Iron Formation (the average is 7.5 ± 2.7 ‰, n = 26; Fig.
653 4). The lower δ¹⁵N values of the Mount McRae Shale might reflect a stronger contribution of N₂-
654 fixation with respect to NO₃⁻ or NH₄⁺ assimilation, lowering δ¹⁵N values towards 0 ‰ (Zerkle et al.,
655 2008), which is characteristic of marine areas with high organic productivity. In contrast, a lower

656 organic productivity at the depositional site of the Brockman Iron Formation would have left
657 more dissolved NO_3^- or NH_4^+ available for assimilation, resulting in less intense N_2 -fixation and
658 higher $\delta^{15}\text{N}$ values of the biomass. In the following sections, the three cases will be further
659 explored and their applicability to the Mount McRae Shale and Brockman Iron Formation will be
660 evaluated.

661

662 *5.4.1. Nitrogen cycle in fully anoxic and ferruginous ocean*

663

664 Under fully anoxic conditions (Fig. 8), dissolved NH_4^+ would accumulate in the water
665 column and would be readily assimilated by living organisms. Ammonium assimilation favours
666 light N isotope, rendering the residual NH_4^+ enriched in ^{15}N (Papineau et al., 2009; Hadas et al.,
667 2009). Assuming a maximum fractionation factor of 27 ‰ for NH_4^+ assimilation (Sigman et al.,
668 2009) and an initial ammonium $\delta^{15}\text{N}$ value of 0 ‰, a Rayleigh distillation model requires that
669 70% of the initial ammonium has to be assimilated and transferred to the sediment before
670 producing organic matter with $\delta^{15}\text{N}$ values of +5 ‰, similar to those found in the Mount McRae
671 Shale and Brockman Iron Formation (Fig. 4). However, the cumulated fraction of organic matter
672 with nitrogen assimilated via such a distillation process would have a mean $\delta^{15}\text{N}$ value around -20
673 ‰, which is not found in either the Mount McRae Shale or Brockman Iron Formation. Thus,
674 partial assimilation of ammonium (case 1 hypothesis) is unlikely to explain the present results.

675 The second hypothesis is based on a partial oxidation of NH_4^+ , followed by complete
676 removal of the nitrite product (Thomazo et al., 2011). Partial oxidation of NH_4^+ leads to the
677 production of isotopically light nitrite with a fractionation of 10 to 40 ‰ (Casciotti et al., 2003),
678 while residual NH_4^+ becomes progressively enriched in heavy isotope. The light isotope is then

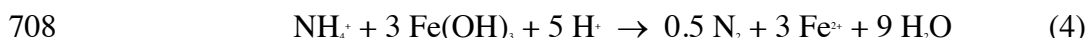
679 removed from the system by quantitative denitrification of nitrite to nitrogen gas (N_2). This
680 sequence of reactions occurs under anoxic conditions, but requires a flux of O_2 that is fully used
681 up. This is rarely observed in modern environments because of their highly oxygenated state.
682 However, a recent study of particulate organic matter in Lake Kinneret, Israel, found ^{15}N -
683 enrichment up to 15-30 ‰ due to partial nitrification of NH_4^+ (Hadas et al., 2009), demonstrating
684 the feasibility of this process. If the positive $\delta^{15}N$ values observed in the Mount McRae Shale and
685 Brockman Iron Formation are inherited from partial oxidation of NH_4^+ , then this process also has
686 to explain the $\delta^{15}N$ - $\delta^{13}C_{carb}$ co-variations observed along the chemostratigraphic profile (Fig. 4). One
687 possibility is that O_2 produced by oxygenic photosynthesis was utilized for both Fe oxidation and
688 partial NH_4^+ oxidation. If this is the case, the flux of Fe-oxyhydroxides, leading to organic matter
689 mineralization and Fe-carbonate precipitation, will roughly correspond with the degree of partial
690 NH_4^+ oxidation. Based on this scenario, an increase in $\delta^{15}N$ values would track an increase in the
691 O_2 production in the upper ocean. It is important to note that application of this model to the
692 open-marine depositional site of the Mount McRae Shale and Brockman Iron Formation requires
693 NH_4^+ stability in the water column and thus generally anoxic conditions, with some “oxygen
694 oases” generated by blooms of oxygenic photosynthesizers (Fig. 8a), inducing partial NH_4^+
695 oxidation.

696 If O_2 was entirely absent from this system, an alternative electron acceptor for NH_4^+
697 oxidation could have been ferric oxyhydroxides ($Fe(OH)_3$ in Fig. 8b) that were generated in
698 anoxic, ferruginous Archean oceans. Microbial oxidation of NH_4^+ with Fe(III) under anaerobic
699 conditions was recently demonstrated in wetland soils (Clément et al., 2005; Shrestha et al.,
700 2009), tropical upland soil slurries (Yang et al., 2012), and a sludge from a cattle waste treatment
701 plant (Sawayama, 2006), and was also shown to be thermodynamically feasible (Clément et al.,

702 2005). This reaction may have been important in the Archean biogeochemical N cycle and can be
703 written as,



705 Following NH_4^+ oxidation, NO_3^- would be reduced to N_2 by denitrification or anammox processes,
706 since it is unstable under anaerobic conditions. Direct NH_4^+ oxidation to N_2 is also energetically
707 feasible, yielding up to 245 kJ/mol (Yang et al., 2012), through the following reaction:



709 Although the N isotope fractionation associated with NH_4^+ oxidation with Fe(III) is not known, it
710 is reasonable to assume fractionations similar to those imposed by O_2 -driven nitrification process
711 (10 to 40 ‰; Casciotti et al., 2003), thus enriching the residual NH_4^+ in ^{15}N . This scenario could
712 also provide an explanation for the roughly inverse trends of $\delta^{15}\text{N}$ and $\delta^{13}\text{C}_{\text{carb}}$ values (Fig. 4). The
713 highest flux of Fe-oxyhydroxides would correspond to the highest rate of ammonium oxidation,
714 resulting in both an increase in $\delta^{15}\text{N}$ values and early diagenetic organic matter mineralization
715 with ferric iron. The latter process in turn would induce Fe-carbonate precipitation with negative
716 $\delta^{13}\text{C}_{\text{carb}}$ values.

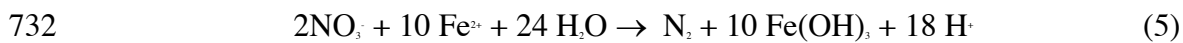
717

718 *5.4.2. Nitrogen cycle in a redox-stratified ocean*

719

720 In the oxic upper layer of a stratified water column (Fig. 8c), NH_4^+ would be quantitatively
721 oxidized to NO_3^- by nitrification, thus preventing any nitrogen isotope fractionation. In oxygen-
722 minimum zones, or at redox boundaries, partial denitrification would increase the $\delta^{15}\text{N}$ value of
723 residual NO_3^- (see review in Sigman et al., 2009). Assimilation of this residual NO_3^- by living
724 organisms would transfer positive N isotope signature to the sedimentary deposit. Such a scenario

725 of a redox-stratified ocean has been proposed in previous studies to explain positive $\delta^{15}\text{N}$ values in
726 Archean sedimentary rocks (Garvin et al., 2009; Godfrey and Falkowski, 2009). This scenario
727 can be extended to the sedimentary sequence of the Brockman Iron Formation if it can explain
728 the coupling between N and Fe biogeochemical cycles in the water column, which is required to
729 establish the $\delta^{15}\text{N}$ - $\delta^{13}\text{C}_{\text{carb}}$ co-variation (Fig. 4). One possibility is that partial denitrification of NO_3^-
730 was mediated by anaerobic microbial oxidation of Fe(II) to Fe(III) (Shen et al., 2006). The
731 corresponding reaction can be written as,



733 The existence of anaerobic nitrate-dependant microbial Fe(II)-oxidation has been demonstrated
734 by laboratory experiments (Straub et al., 1996), but data on N isotope fractionations associated
735 with this process are still lacking. If partial denitrification via this process increases $\delta^{15}\text{N}$ values of
736 residual NO_3^- , as it does in modern marine oxygen-minimum zones (Sigman et al., 2009), then
737 assimilation of the ^{15}N -enriched residual NO_3^- would generate a pool of organic matter with
738 positive $\delta^{15}\text{N}$ values. According to this reaction, the higher fluxes of $\text{Fe}(\text{OH})_3$ to the sediment,
739 possibly inducing diagenetic Fe-carbonate precipitation, would be associated with more positive
740 $\delta^{15}\text{N}$ values in the sedimentary organic matter. Dissolved NO_3^- would be in contact with Fe^{2+} only
741 at the redox boundary between upper oxygenated and lower anoxic layers in a stratified water
742 column (Fig. 8c). Away from the redox boundary, Fe^{2+} would be immediately oxidized to Fe^{3+}
743 under fully oxic conditions, and NO_3^- would be quantitatively denitrified under anoxic conditions.
744 Although redox-stratified water column allows for an inverse relationship between $\delta^{15}\text{N}$ and $\delta^{13}\text{C}_{\text{carb}}$
745 values, as in the Brockman Iron Formation (Fig. 4), the feasibility of this model can be
746 questioned. Based on this scenario, the flux of Fe oxyhydroxides to the sediments has to be
747 balanced by NO_3^- denitrification. The reaction (5) presented above indicates that 1 mole of NO_3^- is

748 required for the oxidation of 5 moles of Fe^{2+} . However, considering the large flux of Fe associated
749 with deposition of banded iron formation, NO_3^- denitrification would have led to extensive,
750 probably quantitative, loss of dissolved NO_3^- to gaseous N_2 . As a result of its low concentration,
751 the residual pool of partially denitrified NO_3^- at the redox boundary would have a negligible
752 impact on the NO_3^- inventory of the upper oxygenated ocean and, more specifically, on the N
753 isotope composition of the NO_3^- -assimilating organisms. The feasibility of this redox-stratified
754 model should be further tested with a detailed dispersion-reaction model coupling N-C-Fe
755 biogeochemical cycles in the water column.

756

757 **6. Conclusion**

758

759 We propose herein that N and Fe biogeochemical cycles in the Late Archean open-marine
760 basin of the Hamersley Province were linked via redox reactions in the water column, and are
761 recorded by inverse co-variations between $\delta^{15}\text{N}$ and $\delta^{13}\text{C}_{\text{carb}}$ values in the Brockman Iron Formation.
762 Like in the Phanerozoic, N was probably introduced to the ocean mainly via N_2 -fixation leading
763 to $\delta^{15}\text{N}$ values close to 0 ‰ in organic matter and NH_4^+ released during mineralization of organic
764 matter. Several scenarios based on different redox structures of the water column can satisfy the
765 literature and our own N isotope data. If the water column was anoxic, NH_4^+ would have been the
766 dominant species of dissolved nitrogen available for assimilation in the photic zone. Positive $\delta^{15}\text{N}$
767 values in this case would represent partial oxidation of NH_4^+ , by either (1) O_2 -controlled
768 nitrification, or (2) microbial oxidation with ferric oxyhydroxides, and subsequent quantitative
769 denitrification of NO_2^- and NO_3^- products. If the water column was redox-stratified, with an oxic
770 layer covering anoxic deep waters, N assimilated by primary producers would have been mostly

771 in the form of NO_3^- like in the Phanerozoic oceans. In this case, the positive $\delta^{15}\text{N}$ values would
772 have been produced by partial denitrification of NO_3^- coupled to anaerobic microbial oxidation of
773 ferrous to ferric iron. Accordingly, similar positive $\delta^{15}\text{N}$ values may record very different N
774 biogeochemical cycles under anoxic, redox-stratified, or fully oxic conditions in the oceans. We
775 emphasize therefore that N isotopes alone cannot be used to constrain the redox structure of the
776 ancient oceans, but can still be useful to address this question if utilized in combination with
777 other elemental and isotopic tracers.

778 As a perspective, we also point out the need to determine experimentally N isotope
779 fractionations associated with microbial redox reactions involving N and Fe cycles, such as NH_4^+
780 oxidation by ferric oxyhydroxides and/or denitrification of NO_3^- mediated by anaerobic oxidation
781 of Fe(II) to Fe(III). This may help future studies for seeking ancient traces of life in the Archean
782 geological record.

783

784 **Acknowledgements**

785 This work was partly funded by the INSU-PNP program of the CNRS and by the BQR grants of
786 IPGP. Colleagues from the Isotope Geochemistry Laboratories in IPGP are thanked for fruitful
787 discussions, particularly Pierre Cartigny, Magali Bonifacie, Pierre Sans-Jofre and Jabrane Labidi.
788 Michel Girard, Jean-Jacques Bourrand, Carine Chaduteau and Guillaume Landais are
789 acknowledged for their technical assistance. Marc Quintin is thanked for making thin sections of
790 all samples. AB contribution was supported by NSF and NSERC Discovery grants. Greame
791 Broadbent from Rio Tinto Exploration is thanked for access to drill cores and geological
792 information. Jim Kasting is thanked for handling the manuscript and three anonymous reviewers

793 are greatly acknowledged for their detailed comments. Contribution IPGP No. XXX and CNRS
794 No. XXX.

795

796 **References**

797

- 798 Ader, M., Boudou, J.P., Javoy, M., Goffe, B. and Daniels, E., 1998. Isotope study on organic
799 nitrogen of Westphalian anthracites from the western middle field of Pennsylvania (USA)
800 and from the Bramsche massif (Germany). *Organic Geochemistry* 29, 315-323.
- 801 Ader, M., Cartigny, P., Boudou, J.P., Oh, J.H., Petit, E. and Javoy, M., 2006. Nitrogen isotopic
802 evolution of carbonaceous matter during metamorphism: Methodology and preliminary
803 results. *Chemical Geology* 232, 152-169.
- 804 Ader, M., Macouin, M., Trindade, R.I.F., Hadrien, M.H., Yang, Z., Sun, Z. and Besse, J., 2009. A
805 multilayered water column in the Ediacaran Yangtze platform? Insights from carbonate
806 and organic matter paired $\delta^{13}\text{C}$. *Earth and Planetary Science Letters* 288, 213-227.
- 807 Alibert, C., and McCulloch, M. T., 1993. Rare element and neodymium isotopic compositions of
808 the banded iron-formations and associated shales from Hamersley, western Australia.
809 *Geochimica Cosmochimica Acta* 57, 187-204.
- 810 Altabet, M.A. and Francois, R., 1994. Sedimentary nitrogen isotopic ratio as a recorder for
811 surface ocean nitrate utilization. *Global Biogeochemical Cycles* 8, 103-116.
- 812 Anbar, A.D., Duan, Y., Lyons, T.W., Arnold, G.L., Kendall, B., Creaser, R.A., Kaufman, A.J.,
813 Gordon, G.W., Scott, C., Garvin, J. and Buick, R., 2007. A whiff of oxygen before the
814 Great Oxidation Event? *Science* 317, 1903-1906.
- 815 Anbar, A.D. and Knoll, A.H., 2002. Proterozoic ocean chemistry and evolution: A bioinorganic
816 bridge? *Science* 297, 1137-1142.
- 817 Beaumont, V. and Robert, F., 1999. Nitrogen isotope ratios of kerogens in Precambrian cherts: a
818 record of the evolution of atmosphere chemistry? *Precambrian Research* 96, 63-82.
- 819 Bebout, G.E., Cooper, D.C., Bradley, A.D. and Sadofsky, S.J., 1999. Nitrogen-isotope record of
820 fluid-rock interactions in the Skiddaw Aureole and granite, English Lake District.
821 *American Mineralogist* 84, 1495-1505.
- 822 Bebout, G.E. and Fogel, M.L., 1992. Nitrogen-isotope compositions of metasedimentary rocks in
823 the Catalina Schist, California - Implications for metamorphic devolatilization history.
824 *Geochimica Et Cosmochimica Acta* 56, 2839-2849.
- 825 Becker, R.H. and Clayton, R.N., 1976. Oxygen isotope study of a Precambrian Banded Iron-
826 Formation, Hamersley Range, Western-Australia. *Geochimica et Cosmochimica Acta* 40,
827 1153-1165.
- 828 Bekker, A., Kaufman, A.J., Karhu, J.A., Beukes, N.J., Swart, Q.D., Coetzee, L.L. and Eriksson,
829 K.A., 2001. Chemostratigraphy of the paleoproterozoic Duitschland Formation, South
830 Africa: Implications for coupled climate change and carbon cycling. *American Journal of*
831 *Science* 301, 261-285.
- 832 Bekker, A., Holland, H.D., Wang, P.L., Rumble, D., Stein, H.J., Hannah, J.L., Coetzee, L.L. and
833 Beukes, N.J., 2004. Dating the rise of atmospheric oxygen. *Nature* 427, 117-120.

- 834 Bekker, A. and Kaufman, A.J., 2007. Oxidative forcing of global climate change: A
835 biogeochemical record across the oldest Paleoproterozoic ice age in North America. *Earth*
836 *and Planetary Science Letters* 258, 486-499.
- 837 Bekker, A., Slack, J.F., Planavsky, N., Krapez, B., Hofmann, A., Konhauser, K.O. and Rouxel,
838 O.J., 2010. Iron Formation: The sedimentary product of a complex interplay among
839 mantle, tectonic, oceanic, and biospheric processes. *Economic Geology* 105, 467-508.
- 840 Beukes, N.J. and Gutzmer, J., 2008. Origin and paleoenvironmental significance of major Iron
841 Formations at the Archean-Paleoproterozoic boundary, Banded Iron Formation-Related
842 High-Grade Iron Ore. *Reviews in Economic Geology*, pp. 5-47.
- 843 Beukes, N.J., Klein, C., Kaufman, A.J. and Hayes, J.M., 1990. Carbonate petrography, kerogen
844 distribution, and carbon and oxygen isotope variations in an Early Proterozoic transition
845 from limestone to iron-formation deposition, Transvaal Supergroup, South-Africa.
846 *Economic Geology* 85, 663-690.
- 847 Blake, T. S. and Barley, M. E., 1992. Tectonic evolution of the Late Archaean to Early Proterozoic
848 Mount Bruce Megasequence Set, Western Australia. *Tectonics* 11, 1415-1425.
- 849 Boudou, J.P., Schimmelmann, A., Ader, M., Mastalerz, M., Sebiló, M. and Gengembre, L., 2008.
850 Organic nitrogen chemistry during low-grade metamorphism. *Geochimica et*
851 *Cosmochimica Acta* 72, 1199-1221.
- 852 Boyd, S.R., 2001. Ammonium as a biomarker in Precambrian metasediments. *Precambrian*
853 *Research* 108, 159-173.
- 854 Brandes, J.A., Devol, A.H. and Deutsch, C., 2007. New developments in the marine nitrogen
855 cycle. *Chemical Reviews* 107, 577-589.
- 856 Busigny, V., Ader, M. and Cartigny, P., 2005. Quantification and isotopic analysis of nitrogen in
857 rocks at the ppm level using sealed tube combustion technique: A prelude to the study of
858 altered oceanic crust. *Chemical Geology* 223, 249-258.
- 859 Busigny, V., Cartigny, P., Philippot, P. and Javoy, M., 2003a. Ammonium quantification in
860 muscovite by infrared spectroscopy. *Chemical Geology* 198, 21-31.
- 861 Busigny, V., Cartigny, P., Philippot, P., Ader, M. and Javoy, M., 2003b. Massive recycling of
862 nitrogen and other fluid-mobile elements (K, Rb, Cs, H) in a cold slab environment:
863 evidence from HP to UHP oceanic metasediments of the Schistes Lustrés nappe (western
864 Alps, Europe). *Earth and Planetary Science Letters* 215, 27-42.
- 865 Canfield, D.E., Glazer, A.N. and Falkowski, P.G., 2010. The evolution and future of Earth's
866 nitrogen cycle. *Science* 330, 192-196.
- 867 Casciotti, K.L., Sigman, D.M. and Ward, B.B., 2003. Linking diversity and stable isotope
868 fractionation in ammonia-oxidizing bacteria. *Geomicrobiology Journal* 20, 335-353.
- 869 Clement, J.C., Shrestha, J., Ehrenfeld, J.G. and Jaffe, P.R., 2005. Ammonium oxidation coupled
870 to dissimilatory reduction of iron under anaerobic conditions in wetland soils. *Soil*
871 *Biology & Biochemistry* 37, 2323-2328.
- 872 Cloud, P., 1973. Paleoeological Significance of Banded Iron-Formation. *Economic Geology* 68,
873 1135-1143.
- 874 Craddock, P.R. and Dauphas, N., 2011. Iron and carbon isotope evidence for microbial iron
875 respiration throughout the Archean. *Earth and Planetary Science Letters* 303, 121-132.
- 876 Dauphas, N., Cates, N.L., Mojzsis, S.J. and Busigny, V., 2007a. Identification of chemical
877 sedimentary protoliths using iron isotopes in the > 3750 Ma Nuvvuagittuq supracrustal
878 belt, Canada. *Earth and Planetary Science Letters* 254, 358-376.

- 879 Dauphas, N., van Zuilen, M., Busigny, V., Lepland, A., Wadhwa, M. and Janney, P.E., 2007b.
880 Iron isotope, major and trace element characterization of early Archean supracrustal rocks
881 from SW Greenland: Protolith identification and metamorphic overprint. *Geochimica et*
882 *Cosmochimica Acta* 71, 4745-4770.
- 883 Fischer, W.W., Schroeder, S., Lacassie, J.P., Beukes, N.J., Goldberg, T., Strauss, H., Horstmann,
884 U.E., Schrag, D.P. and Knoll, A.H., 2009. Isotopic constraints on the Late Archean
885 carbon cycle from the Transvaal Supergroup along the western margin of the Kaapvaal
886 Craton, South Africa. *Precambrian Research* 169, 15-27.
- 887 Garvin, J., Buick, R., Anbar, A.D., Arnold, G.L. and Kaufman, A.J., 2009. Isotopic evidence for
888 an aerobic nitrogen cycle in the latest Archean. *Science* 323, 1045-1048.
- 889 Gaye, B., Wiesner, M.G. and Lahajnar, N., 2009. Nitrogen sources in the South China Sea, as
890 discerned from stable nitrogen isotopic ratios in rivers, sinking particles, and sediments.
891 *Marine Chemistry* 114, 72-85.
- 892 Godfrey, L.V. and Falkowski, P.G., 2009. The cycling and redox state of nitrogen in the
893 Archaean ocean. *Nature Geoscience* 2, 725-729.
- 894 Guo, Q.J., Strauss, H., Kaufman, A.J., Schroder, S., Gutzmer, J., Wing, B., Baker, M.A., Bekker,
895 A., Jin, Q.S., Kim, S.T. and Farquhar, J., 2009. Reconstructing Earth's surface oxidation
896 across the Archean-Proterozoic transition. *Geology* 37, 399-402.
- 897 Hadas, O., Altabet, M.A. and Agnihotri, R., 2009. Seasonally varying nitrogen isotope
898 biogeochemistry of particulate organic matter in Lake Kinneret, Israel. *Limnology and*
899 *Oceanography* 54, 75-85.
- 900 Hayes, J.M., Kaplan, I.R. and Wedeking, W., 1983. Geochemical evidence bearing on the origin
901 of aerobiosis, a speculative hypothesis. In: S.J. W. (Editor), *Earth's earliest biosphere, its*
902 *origin and evolution*. Princeton University Press, Princeton.
- 903 Hayes, J. M., Strauss, H., and Kaufman, A. J., 1999. The abundance of ^{13}C in marine organic
904 matter and isotopic fractionation in the global biogeochemical cycle of carbon during the
905 past 800 Ma. *Chemical Geology* 161, 103-125.
- 906 Heimann, A., Johnson, C.M., Beard, B.L., Valley, J.W., Roden, E.E., Spicuzza, M.J. and Beukes,
907 N.J., 2010. Fe, C, and O isotope compositions of banded iron formation carbonates
908 demonstrate a major role for dissimilatory iron reduction in similar to 2.5 Ga marine
909 environments. *Earth and Planetary Science Letters* 294, 8-18.
- 910 Holland, H.D., 1984. *The chemical evolution of the atmosphere and oceans*. Princeton University
911 Press, Princeton, 582 pp.
- 912 Holland, H.D., 2002. Volcanic gases, black smokers, and the Great Oxidation Event. *Geochimica*
913 *Et Cosmochimica Acta* 66, 3811-3826.
- 914 Holland, H.D., 2006. The oxygenation of the atmosphere and oceans. *Philosophical Transactions*
915 *of the Royal Society B* 361, 903-915.
- 916 Holland, H.D., 2009. Why the atmosphere became oxygenated: A proposal. *Geochimica Et*
917 *Cosmochimica Acta* 73, 5241-5255.
- 918 Honma, H. and Itihara, Y., 1981. Distribution of ammonium in minerals of metamorphic and
919 granitic-rocks. *Geochimica Et Cosmochimica Acta* 45, 983-988.
- 920 Jia, Y.F., 2006. Nitrogen isotope fractionations during progressive metamorphism: A case study
921 from the Paleozoic Cooma metasedimentary complex, southeastern Australia.
922 *Geochimica Et Cosmochimica Acta* 70, 5201-5214.
- 923 Jia, Y.F. and Kerrich, R., 2004a. A reinterpretation of the crustal N-isotope record: evidence for a
924 N-15-enriched Archean atmosphere? *Terra Nova* 16, 102-108.

- 925 Jia, Y.F. and Kerrich, R., 2004b. Nitrogen 15-enriched Precambrian kerogen and hydrothermal
926 systems. *Geochemistry Geophysics Geosystems* 5, Q07005, doi:10.1029/2004GC000716.
- 927 Junium, C.K., and Arthur, M.A., 2007. Nitrogen cycling during the Cretaceous, Cenomanian-
928 Turonian Oceanic Anoxic Event II. *Geochemistry Geophysics Geosystems* 8, Q03002,
929 doi:10.1029/2006GC001328
- 930 Kappler, A., Pasquero, C., Konhauser, K.O. and Newman, D.K., 2005. Deposition of banded iron
931 formations by anoxygenic phototrophic Fe(II)-oxidizing bacteria. *Geology* 33, 865-868.
- 932 Kaufman, A.J., Hayes, J.M. and Klein, C., 1990. Primary and diagenetic controls of isotopic
933 compositions of iron-formation carbonates. *Geochimica et Cosmochimica Acta* 54, 3461-
934 3473.
- 935 Kaufman, A.J., Johnston, D.T., Farquhar, J., Masterson, A.L., Lyons, T.W., Bates, S., Anbar,
936 A.D., Arnold, G.L., Garvin, J. and Buick, R., 2007. Late Archean biospheric oxygenation
937 and atmospheric evolution. *Science* 317, 1900-1903.
- 938 Kendall, C. and Grim, E., 1990. Combustion tube method for measurement of nitrogen isotope
939 ratios using calcium-oxide for total removal of carbon-dioxide and water. *Analytical*
940 *Chemistry* 62, 526-529.
- 941 Konhauser, K.O., Hamade, T., Raiswell, R., Morris, R.C., Ferris, F.G., Southam, G. and
942 Canfield, D.E., 2002. Could bacteria have formed the Precambrian banded iron
943 formations? *Geology* 30, 1079-1082.
- 944 Krapež, B., Barley, M.E. and Pickard, A.L., 2003. Hydrothermal and re-sedimented origins of the
945 precursor sediments to banded iron formation: sedimentological evidence from the Early
946 Palaeoproterozoic Brockman Supersequence of Western Australia. *Sedimentology* 50,
947 979-1011.
- 948 Lehmann, M.F., Bernasconi, S.M., Barbieri, A. and McKenzie, J.A., 2002. Preservation of
949 organic matter and alteration of its carbon and nitrogen isotope composition during
950 simulated and in situ early sedimentary diagenesis. *Geochimica et Cosmochimica Acta*
951 66, 3573-3584.
- 952 Marty, B., Zimmermann, L., Pujol, M., Burgess, R. and Philippot, P., 2012. Nitrogen
953 composition of the ancient atmosphere from fluid inclusion analysis of Archean quartz.
954 *Mineralogical Magazine, Goldschmidt Conference Abstracts*, p. 65.
- 955 McCrea, J.M., 1950. On the isotopic chemistry of carbonates and a paleotemperature scale.
956 *Journal of Chemical Physics* 18, 849-857.
- 957 Minagawa, M. and Wada, E., 1986. Nitrogen isotope ratios of red tide organisms in the East-
958 China sea - a characterization of biological nitrogen-fixation. *Marine Chemistry* 19, 245-
959 259.
- 960 Mingram, B. and Brauer, K., 2001. Ammonium concentration and nitrogen isotope composition
961 in metasedimentary rocks from different tectonometamorphic units of the European
962 Variscan Belt. *Geochimica et Cosmochimica Acta* 65, 273-287.
- 963 Miyano, T. and Klein, C., 1989. Phase-equilibria in the system K₂O-FeO-MgO-Al₂O₃-SiO₂-
964 H₂O-CO₂ and the stability limit of stilpnomelane in metamorphosed precambrian iron-
965 formations. *Contributions to Mineralogy and Petrology* 102, 478-491.
- 966 Möbius, J., Lahajnar, N. and Emeis, K.C., 2010. Diagenetic control of nitrogen isotope ratios in
967 Holocene sapropels and recent sediments from the Eastern Mediterranean Sea.
968 *Biogeosciences* 7, 3901-3914.

- 969 Möbius, J., 2013. Isotope fractionation during nitrogen remineralization (ammonification):
970 Implications for nitrogen isotope biogeochemistry. *Geochimica et Cosmochimica Acta*
971 105, 422-432.
- 972 Morse, J.W. and Mackenzie, F.T., 1990. *Geochemistry of sedimentary carbonates. Developments*
973 *in sedimentology* 48. Elsevier, 681 pp.
- 974 Murakami, T., Sreenivas, B., Das Sharma, S. and Sugimori, H., 2011. Quantification of
975 atmospheric oxygen levels during the Paleoproterozoic using paleosol compositions and
976 iron oxidation kinetics. *Geochimica Et Cosmochimica Acta* 75, 3982-4004.
- 977 Papineau, D., Mojzsis, S.J., Karhu, J.A. and Marty, B., 2005. Nitrogen isotopic composition of
978 ammoniated phyllosilicates: case studies from Precambrian metamorphosed sedimentary
979 rocks. *Chemical Geology* 216, 37-58.
- 980 Papineau, D., Purohit, R., Goldberg, T., Pi, D.H., Shields, G.A., Bhu, H., Steele, A. and Fogel,
981 M.L., 2009. High primary productivity and nitrogen cycling after the Paleoproterozoic
982 phosphogenic event in the Aravalli Supergroup, India. *Precambrian Research* 171, 37-56.
- 983 Pecoits, E., Gingras, M.K., Barley, M.E., Kappler, A., Posth, N.R. and Konhauser, K.O., 2009.
984 Petrography and geochemistry of the Dales Gorge banded iron formation: Paragenetic
985 sequence, source and implications for palaeo-ocean chemistry. *Precambrian Research*
986 172, 163-187.
- 987 Pickard, A.L., Barley, M.E. and Krapez, B., 2004. Deep-marine depositional setting of banded
988 iron formation: sedimentological evidence from interbedded clastic sedimentary rocks in
989 the early Palaeoproterozoic Dales Gorge Member of Western Australia. *Sedimentary*
990 *Geology* 170, 37-62.
- 991 Pinti, D.L. and Hashizume, K., 2001. ¹⁵N-depleted nitrogen in Early Archean kerogens: clues on
992 ancient marine chemosynthetic-based ecosystems? A comment to Beaumont, V.,
993 Robert, F., 1999. *Precambrian Res.* 96, 62-82. *Precambrian Research* 105, 85-88.
- 994 Pinti, D.L., Hashizume, K. and Matsuda, J., 2001. Nitrogen and argon signatures in 3.8 to 2.8 Ga
995 metasediments: Clues on the chemical state of the Archean ocean and the deep biosphere.
996 *Geochimica Et Cosmochimica Acta* 65, 2301-2315.
- 997 Pinti, D.L., Hashizume, K., Orberger, B., Gallien, J.P., Cloquet, C. and Massault, M., 2007.
998 Biogenic nitrogen and carbon in Fe-Mn-oxyhydroxides from an Archean chert, Marble
999 Bar, Western Australia. *Geochemistry Geophysics Geosystems* 8.
- 1000 Pinti, D.L., Hashizume, K., Sugihara, A., Massault, M. and Philippot, P., 2009. Isotopic
1001 fractionation of nitrogen and carbon in Paleoarchean cherts from Pilbara craton, Western
1002 Australia: Origin of N-15-depleted nitrogen. *Geochimica et Cosmochimica Acta* 73,
1003 3819-3848.
- 1004 Planavsky, N., Bekker, A., Rouxel, O.J., Kamber, B., Hofmann, A., Knudsen, A. and Lyons,
1005 T.W., 2010. Rare Earth Element and yttrium compositions of Archean and
1006 Paleoproterozoic Fe formations revisited: New perspectives on the significance and
1007 mechanisms of deposition. *Geochimica et Cosmochimica Acta* 74, 6387-6405.
- 1008 Prokopenko, M.G., Hammond, D.E., Berelson, W.M., Bernhard, J.M., Stott, L. and Douglas, R.,
1009 2006. Nitrogen cycling in the sediments of Santa Barbara basin and Eastern Subtropical
1010 North Pacific: Nitrogen isotopes, diagenesis and possible chemosymbiosis between two
1011 lithotrophs (*Thioploca* and *Anammox*) - "riding on a glider". *Earth and Planetary Science*
1012 *Letters* 242, 186-204.
- 1013 Raiswell, R., Reinhard, C.T., Derkowski, A., Owens, J., Bottrell, S.H., Anbar, A.D. and Lyons,
1014 T.W., 2011. Formation of syngenetic and early diagenetic iron minerals in the late

- 1015 Archean Mt. McRae Shale, Hamersley Basin, Australia: New insights on the patterns,
1016 controls and paleoenvironmental implications of authigenic mineral formation.
1017 *Geochimica et Cosmochimica Acta* 75, 1072-1087.
- 1018 Rasmussen, B., Meier, D.B., and Krapež, B., 2013. Iron silicate microgranules as precursor
1019 sediments to 2.5-billion-year-old banded iron formations. *Geology* 41, 435-438.
- 1020 Rasmussen, B., Blake, T.S. and Fletcher, I.R., 2005. U-Pb zircon age constraints on the
1021 Hamersley spherule beds: Evidence for a single 2.63 Ga Jeerinah-Carawine impact ejecta
1022 layer. *Geology* 33, 725-728.
- 1023 Rau, G.H., Arthur, M.A., and Dean, W.E., 1987. $^{15}\text{N}/^{14}\text{N}$ variations in Cretaceous Atlantic
1024 sedimentary sequences: implication for past changes in marine nitrogen biogeochemistry.
1025 *Earth and Planetary Science Letters* 82, 269-279.
- 1026 Reinhard, C.T., Raiswell, R., Scott, C., Anbar, A.D. and Lyons, T.W., 2009. A late Archean
1027 sulfidic sea stimulated by early oxidative weathering of the continents. *Science* 326, 713-
1028 716.
- 1029 Rosenbaum, J. and Sheppard, S.M.F., 1986. An isotopic study of siderites, dolomites and
1030 ankerites at high-temperatures. *Geochimica et Cosmochimica Acta* 50, 1147-1150.
- 1031 Rouchon, V., Pinti, D.L., Gallien, J.P., Orberger, B., Daudin, L., and Westall, F. (2005) NRA
1032 analyses of N and C in hydromuscovite aggregates from a 3.5 Ga chert from Kittys Gap,
1033 Pilbara, Australia. *Nuclear Instruments and Methods in Physics Research B* 231, 536-
1034 540.
- 1035 Sansjofre, P., Ader, M., Trindade, R.I.F., Elie, M., Lyons, J., Cartigny, P. and Nogueira, A.C.R.,
1036 2011. A carbon isotope challenge to the Snowball Earth. *Nature* 478, 93-97.
- 1037 Sawayama, S., 2006. Possibility of anoxic ferric ammonium oxidation. *Journal of Bioscience and*
1038 *Bioengineering* 101, 70-72.
- 1039 Scott, C.T., Bekker, A., Reinhard, C.T., Schnetger, B., Krapez, B., Rumble, D. and Lyons, T.W.,
1040 2011. Late Archean euxinic conditions before the rise of atmospheric oxygen. *Geology*
1041 39, 119-122.
- 1042 Shen, Y., Pinti, D.L., and Hashizume, K., 2006. Biogeochemical cycles of sulfur and nitrogen in
1043 the Archean ocean and atmosphere. In: K. Benn, J.C. Mareschal and K.C. Condie
1044 (Editors), *Archean Geodynamics and Environments*. American Geophysical Union,
1045 Washington D.D. *Geophysical Monograph* 164, 305-320.
- 1046 Shrestha, J., Rich, J.J., Ehrenfeld, J.G. and Jaffe, P.R., 2009. Oxidation of ammonium to nitrite
1047 under iron-reducing conditions in wetland soils laboratory, field demonstrations, and
1048 push-pull rate determination. *Soil Science* 174, 156-164.
- 1049 Sigman, D.M., Karsh, K.L. and Casciotti, K.L., 2009. Nitrogen isotopes in the ocean. In: J.H.
1050 Steele, T. S.A. and K.K. Turekian (Editors), *Encyclopedia of Ocean Sciences*. Academic
1051 Press, Oxford, pp. 40-54.
- 1052 Smith, R. E., Perdrix, J. L., and Parks, T. C., 1982. Burial metamorphism in the Hamersley Basin,
1053 Western Australia. *Journal of Petrology* 23, 75-102.
- 1054 Straub, K.L., Benz, M., Schink, B., and Widdel, F., 1996. Anaerobic, nitrate dependent microbial
1055 oxidation of ferrous iron. *Applied and Environmental Microbiology* 62, 1458-1460.
- 1056 Thomazo, C., Ader, M., Farquhar, J. and Philippot, P., 2009a. Methanotrophs regulated
1057 atmospheric sulfur isotope anomalies during the Mesoarchean (Tumbiana Formation,
1058 Western Australia). *Earth and Planetary Science Letters* 279, 65-75.
- 1059 Thomazo, C., Pinti, D.L., Busigny, V., Ader, M., Hashizume, K. and Philippot, P., 2009b.
1060 Biological activity and the Earth's surface evolution: Insights from carbon, sulfur,

1061 nitrogen and iron stable isotopes in the rock record. *Comptes Rendus Palevol* 8, 665-
1062 678.

1063 Thomazo, C., Ader, M. and Philippot, P., 2011. Extreme ¹⁵N-enrichments in 2.72-Gyr-old
1064 sediments: evidence for a turning point in the nitrogen cycle. *Geobiology* 9, 107-120.

1065 Thunell, R.C., Sigman, D.M., Muller-Karger, F., Astor, Y. and Varela, R., 2004. Nitrogen isotope
1066 dynamics of the Cariaco Basin, Venezuela. *Global Biogeochemical Cycles* 18.

1067 Tolstikhin, I.N. and Marty, B., 1998. The evolution of terrestrial volatiles: a view from helium,
1068 neon, argon and nitrogen isotope modelling. *Chemical Geology* 147, 27-52.

1069 Trendall, A.F. and Blockley, J.G., 1970. The iron formations of the Precambrian Hamersley
1070 Group of Western Australia, with special reference to crocidolite. *Bull. Geol. Surv. West.*
1071 *Aust.* 119, 366 pp.

1072 Trendall, A.F., Compston, W., Nelson, D.R., De Laeter, J.R. and Bennett, V.C., 2004. SHRIMP
1073 zircon ages constraining the depositional chronology of the Hamersley Group, Western
1074 Australia. *Australian Journal of Earth Sciences* 51, 621-644.

1075 Ueno, Y., Yoshioka, H., Maruyama, S. and Isosaki, Y., 2004. Carbon isotopes and Petrography
1076 of kerogens in ~3.5-Ga hydrothermal silica dikes in the North Pole area, Western
1077 Australia. *Geochimica et Cosmochimica Acta* 68, 573-589.

1078 Wada, E., Kadonaga, T. and Matsuo, S., 1975. ¹⁵N abundance in nitrogen of naturally occurring
1079 substances and global assessment of denitrification from isotopic viewpoint. *Geochemical*
1080 *Journal* 9, 139-148.

1081 Walker, J.C.G., 1984. Suboxic Diagenesis in Banded Iron Formations. *Nature* 309, 340-342.

1082 Webb, A.D., Dickens, G.R. and Oliver, N.H.S., 2003. From banded iron-formation to iron ore:
1083 geochemical and mineralogical constraints from across the Hamersley Province, Western
1084 Australia. *Chemical Geology* 197, 215-251.

1085 Yang, W.H., Weber, K.A. and Silver, W.L., 2012. Nitrogen loss from soil through anaerobic
1086 ammonium oxidation coupled to iron reduction. *Nature Geoscience* 5, 538-541.

1087 Zerkle, A.L., Junium, C.K., Canfield, D.E. and House, C.H., 2008. Production of ¹⁵N-depleted
1088 biomass during cyanobacterial N₂-fixation at high Fe concentrations. *Journal of*
1089 *Geophysical Research-Biogeosciences* 113, G03014, doi:10.1029/2007JG000651.

1090 Zhang, C.L., Horita, J., Cole, D.R., Zhou, J., Lovley, D.R. and Phelps, T.J., 2001. Temperature-
1091 dependant oxygen and carbon isotope fractionations of biogenic siderite. *Geochimica et*
1092 *Cosmochimica Acta* 65, 2257-2271.

1093

1094

1095

1096

Table 1

Stratigraphic unit, depth in the drill core, rock type and mineralogical description of the samples from the Mount McRae Shale and Brockman Iron Formation analyzed in this study.

Stratigraphic unit	Sample #	Depth, m	Rock type	Mineralogy
<i>Brockman Iron Formation</i>				
Joffre Member	J1-124-1	124.7	stilp-rich mudrock	stilp, qtz, K-fdsp, carb (5%), chl, sulfide
Joffre Member	J1-138-1	138.7	calcareous stilp-rich mudrock	stilp, qtz, K-fdsp, carb (30%), chl, sulfide
Joffre Member	J1-148-2	148.2	calcareous stilp-rich mudrock	Fe-carb (37%; siderite), stilp, biot, minor chl, sulfide
Joffre Member	J1-148-3	148.2	stilp-rich mudrock	stilp, sulfide, carb (3%)
Joffre Member	J1-162-1	162	stilp-rich mudrock	stilp, qtz, fdsp, sulfide*
Whaleback Shale	WS188	188	stilp-rich mudrock	stilp, qtz, fdsp, chl, biot, carb (9%)
Whaleback Shale	WS196	196.8	calcareous stilp-rich mudrock	stilp, carb (30%), K-fdsp, qtz, rare biot, sulfide
Dales Gorge Member	DGM236	236.6	calcareous stilp-rich mudrock	stilp, carb (40%), qtz, fdsp, chl, biot, rare sulfide
Dales Gorge Member	DGM243	243	calcareous stilp-rich mudrock	K-fdsp, biot, qtz, stilp, carb (20%), rare sulfide
Dales Gorge Member	DGM258-1	258.3	calcareous stilp-rich mudrock	stilp, carb (25%), Fe-ox, rare biot, sulfide
Dales Gorge Member	DGM258-2	258.3	calcareous stilp-rich mudrock	stilp, carb (45%), Fe-ox, rare biot, sulfide
Dales Gorge Member	DGM268	268.8	calcareous stilp-rich mudrock	stilp, carb (14%), minor qtz, fdsp, sulfide
Dales Gorge Member	DGM271-2	271.8	stilp-rich mudrock	stilp (40%), chl (60%)
Dales Gorge Member	DGM287	287	calcareous stilp-rich mudrock	qtz, K-fdsp, biot, carb (10%), chl, org. mat., sulfide
Dales Gorge Member	DGM288-1	288	calcareous stilp-rich mudrock	stilp, Fe-carb (53%, siderite)
Dales Gorge Member	DGM288-2	288	BIF	chert, carb (83%, siderite)
Dales Gorge Member	DGM302	302.6	calcareous stilp-rich mudrock	Fe-carb (42%), stilp, biot, minor chl, sulfide
Dales Gorge Member	DGM307-4	307.9	BIF	Fe-ox, carb (20%), minor stilp, sulfide
Dales Gorge Member	DGM307-6	307.9	Fe-carb-rich chert	chert, carb (23%, ankerite)
Dales Gorge Member	DGM325	325.6	calcareous stilp-rich mudrock	stilp, chl, biot, carb (20%), sulfide
Dales Gorge Member	DGM337	337.9	calcareous stilp-rich mudrock	stilp, chl, biot, carb (30%, ferroan dolomite), sulfide
Dales Gorge Member	DGM350	350.85	stilp-rich mudrock	stilp, qtz, chl, K-fdsp, carb (10%)
<i>Mount McRae Shale</i>				
Colonial Chert	CC364	364	BIF	Fe-ox, Fe-carb (35%; siderite), minor stilp, chl, sulfide
Colonial Chert	CC367	367.7	calcareous stilp-rich mudrock	stilp, chl, carb (11%), minor fdsp, sulfide
Colonial Chert	CC373	373.9	stilp-rich mudrock	stilp, chl, carb (8%), minor fdsp, sulfide
Colonial Chert	CC376	376.5	stilp-rich mudrock	stilp, chl, carb (3%), minor fdsp
Mc Rae Shale	MR379	379.9	organic-rich marl	carb (40%; dolomite), qtz, K-fdsp, biot, org. mat., sulfide
Mc Rae Shale	MR381	381	organic-rich marl	carb (50%; dolomite), qtz, K-fdsp, biot, org. mat., sulfide
Mc Rae Shale	MR382	382.3	calcareous black shale	qtz, K-fdsp, biot, carb (8%; dolomite), org. mat., sulfide
Mc Rae Shale	MR383	383.8	organic-rich marl	carb (60%; dolomite), qtz, K-fdsp, biot, org. mat., sulfide
Mc Rae Shale	MR387	387.4	organic-rich marl	carb (60%; dolomite), qtz, K-fdsp, biot, org. mat., sulfide

Column 4 includes 4 types of rocks : organic-rich marls, stilpnomelane-rich mudrocks, calcareous (i.e. >10% carb) stilpnomelane-rich mudrocks, banded iron formation (BIF), and one chert rich in Fe-carbonates.

Column 5: mineralogy from thin section and SEM analyses. The values in brackets indicate the proportion of carbonates as determined from H₂PO₄ decarbonation (see details in the analytical section). Abbreviations: stilp: stilpnomelane; qtz: quartz; K-fdsp: potassic feldspar; carb: carbonates; chl: chlorite; biot: biotite; Fe-ox: Fe-oxides (hematite and/or magnetite), org. mat.: high organic matter content; Fe-carb: Fe-rich carbonate.

Table 2

Major element concentrations in samples from the Mount McRae Shale and Brockman Iron Formation (in wt.%).

Sample #	SiO ₂	Al ₂ O ₃	Fe ₂ O ₃	MnO	MgO	CaO	Na ₂ O	K ₂ O	TiO ₂	P ₂ O ₅	LOI	Total
J1-124-1	55.02	12.72	14.51	0.03	2.62	1.14	0.25	11.36	0.08	0.05	2.78	100.55
J1-138-1	30.02	2.99	41.38	0.64	5.67	0.44	0.41	1.47	0.09	0.08	17.11	100.31
J1-148-3	44.14	4.85	35.21	0.12	5.44	0.28	0.70	2.48	0.14	0.07	7.00	100.41
J1-148-2	25.02	2.99	41.98	0.60	6.79	1.28	0.38	1.54	0.07	0.07	19.72	100.44
J1-162-1	45.57	6.72	31.45	0.05	5.85	0.04	0.59	3.90	0.12	0.07	6.19	100.53
WS188	36.29	9.25	31.22	0.16	6.82	1.39	0.27	4.26	0.16	0.31	9.80	99.93
WS196	33.56	7.85	19.78	0.33	6.11	9.41	0.26	5.90	0.34	0.11	15.78	99.44
DGM236	29.59	5.29	28.57	0.53	5.51	6.04	0.18	4.06	0.17	0.13	19.24	99.30
DGM243	46.38	12.46	11.21	0.22	3.66	5.77	0.11	10.48	0.26	0.10	9.98	100.63
DGM258-1	29.37	3.14	43.02	0.47	5.20	0.81	0.27	2.33	0.11	0.09	14.49	99.30
DGM258-2	23.10	2.71	38.85	0.57	5.94	5.68	0.21	2.00	0.14	0.07	19.85	99.11
DGM268	37.66	7.29	26.23	0.36	7.79	4.27	0.67	2.91	0.32	0.13	12.22	99.84
DGM271-2	29.53	15.37	35.16	0.07	11.54	-	0.14	0.51	0.17	0.06	7.67	100.21
DGM287	51.28	12.40	13.24	0.13	5.94	3.04	-	5.60	0.50	0.17	8.37	100.65
DGM288-1	14.01	1.38	45.55	0.73	9.18	1.92	0.23	0.62	0.03	0.18	26.47	100.29
DGM288-2	8.96	0.74	43.81	0.86	10.53	2.40	0.13	0.37	0.01	0.24	31.11	99.16
DGM302	24.53	2.38	45.34	0.29	5.65	1.07	0.45	0.97	0.09	0.11	19.85	100.73
DGM307-4	14.26	1.42	64.78	0.18	3.75	4.20	0.29	0.56	0.03	1.95	9.64	101.06
DGM307-6	73.13	0.19	6.71	0.11	2.32	6.86	-	0.05	0.00	-	10.53	99.90
DGM325	33.24	4.38	37.21	0.37	5.87	2.18	0.76	1.67	0.21	0.09	14.11	100.08
DGM337	29.06	6.63	26.82	0.12	8.95	8.80	0.69	1.09	0.29	0.08	17.90	100.43
DGM350	49.65	3.43	25.88	0.13	7.32	0.67	0.65	1.29	0.01	0.07	9.97	99.05
CC364	4.56	0.18	78.16	0.13	3.12	3.19	-	0.12	0.01	0.17	10.54	100.19
CC367	34.64	7.77	29.92	0.08	10.09	3.09	0.53	1.07	0.28	0.11	12.13	99.70
CC373	37.77	6.68	31.94	0.05	9.34	0.65	0.71	1.38	0.24	0.08	10.34	99.18
CC376	38.67	7.90	30.37	0.04	10.77	0.63	0.64	1.37	0.29	0.09	8.71	99.48
MR379	35.82	9.58	6.19	0.28	8.33	13.15	-	4.98	0.33	0.06	21.31	100.03
MR381	31.89	7.71	4.60	0.38	8.44	16.53	-	4.51	0.27	0.05	24.94	99.34
MR382	59.32	14.03	2.31	0.07	2.94	2.35	0.21	9.34	0.46	0.07	8.75	99.85
MR383	29.01	8.71	2.71	0.39	10.37	16.77	0.11	6.03	0.12	0.03	26.32	100.55
MR387	27.90	7.55	3.28	0.28	10.18	17.55	-	3.91	0.23	0.04	29.21	100.13

Table 3

Carbonate and organic carbon contents and their C isotopic compositions, bulk N content and its isotopic composition, C/N and Fe/Ti molar ratios in samples from the Mount McRae Shale and Brockman Iron Formation

Sample #	C _{carb 40°C} , wt%	C _{carb 130°C} , wt%	C _{carb total} , wt%	δ ¹³ C _{carb total} , ‰	C _{org} , wt%	δ ¹³ C _{org} , ‰	N _{bulk} , ppm	δ ¹⁵ N, ‰	C _{org} /N _{bulk}	Fe/Ti
J1-124-1	4.4	bdl	4.4	-8.6	0.14	-28.27	87.4	9.5	18.9	188.4
J1-138-1	11.7	21.3	33.1	-8.6	0.41	-28.70	16.7	8.1	285.9	465.0
J1-148-3	1.5	1.7	3.2	-7.9	0.52	-28.64	46.5	9.5	129.9	258.9
J1-148-2	12.4	24.5	36.9	-8.3	0.35	-28.22	40.3	8.6	102.5	617.4
J1-162-1	0.1	bdl	0.1	bdl	0.28	-28.74	121.3	7.4	26.7	273.5
WS188	4.6	3.9	8.5	-7.8	0.66	-28.98	8.6	5.1	894.6	200.1
WS196	32.5	bdl	32.5	-5.1	0.42	-27.62	173.3	6.0	28.4	58.4
DGM236	25.2	14.7	39.9	-8.1	0.70	-28.34	54.0	9.0	150.4	167.1
DGM243	17.9	bdl	17.9	-9.3	0.93	-29.04	100.0	9.2	108.8	43.6
DGM258-1	11.6	15.0	26.6	-7.4	0.49	-28.48	63.2	13.4	90.5	384.1
DGM258-2	29.8	16.2	46.0	-7.2	1.06	-28.61	62.8	11.6	196.2	285.7
DGM268	13.3	1.0	14.3	-5.5	1.39	-29.24	113.9	4.2	142.7	81.5
DGM271-2	0.1	bdl	0.1	bdl	0.67	-28.62	31.2	7.6	250.6	204.4
DGM287	9.7	bdl	9.7	-6.1	1.93	-31.29	186.1	4.8	120.9	26.5
DGM288-1	21.5	31.7	53.1	-7.0	1.44	-29.95	40.6	0.4	415.0	1469.3
DGM288-2	-	83.3	83.3	-6.8	1.20	-28.92	6.2	5.8	2250.9	5475.9
DGM302	24.7	18.2	42.9	-8.0	0.28	-28.70	6.0	6.3	547.3	487.5
DGM307-4	14.7	6.7	21.3	-7.9	0.18	-28.29	6.0	8.0	348.4	2491.4
DGM307-6	22.7	bdl	22.7	-7.8	0.05	-26.43	1.3	7.9	421.4	1678.0
DGM325	11.8	11.3	23.1	-9.0	0.29	-28.76	24.2	8.8	138.7	179.8
DGM337	29.6	2.0	31.6	-9.2	0.41	-28.41	10.7	9.9	443.5	94.1
DGM350	4.4	5.8	10.1	-10.7	0.22	-29.22	7.6	11.1	345.1	2876.0
CC364	20.4	15.2	35.6	-9.2	0.59	-28.16	83.9	6.7	81.5	7816.4
CC367	9.1	1.2	10.3	-5.9	1.22	-28.48	38.8	3.2	367.4	105.4
CC373	3.7	4.6	8.3	-9.2	0.70	-28.85	30.4	7.0	267.0	133.1
CC376	1.7	1.2	2.9	-10.5	0.62	-28.63	61.7	6.9	117.8	104.7
MR379	40.0	bdl	40.0	-4.2	1.74	-28.83	384.7	5.4	52.8	18.5
MR381	51.1	bdl	51.1	-3.9	2.64	-28.59	385.5	5.7	80.0	16.9
MR382	8.0	bdl	8.0	-3.7	3.05	-29.39	785.5	4.4	45.2	5.1
MR383	56.0	bdl	56.0	-3.2	1.92	-29.15	497.5	4.4	45.0	23.5
MR387	57.9	bdl	57.9	-5.6	4.58	-30.48	420.1	4.6	127.2	14.2

bdl: below detection limit.

C_{org}/N_{bulk} and Fe/Ti are molar ratios.

1097 **Figure captions**

1098
1099 **Fig. 1.** Geological map of the Hamersley Province and stratigraphic divisions of the upper part of
1100 the Hamersley Group showing the location of the drill-core WLT-10 and stratigraphic position of
1101 the geological units discussed in this work (modified from Krapež et al., 2003). The boundary
1102 between the Chichester Range and Hamersley Range megasequences is the unconformity at the
1103 base of the Mount Sylvia Formation (Blake and Barley, 1992).

1104
1105 **Fig. 2.** Major element concentrations (in wt%) of the samples analyzed in our study, including
1106 organic-rich shales from the Mount McRae Shale, and stilpnomelane-rich mudrocks, banded iron
1107 formations and chert from the Brockman Iron Formation. Samples are marked as "calcareous" if
1108 their total carbonate content is higher than 10 wt%.

1109
1110 **Fig. 3.** Organic carbon content (in wt%) and whole-rock nitrogen content (in ppm) versus Fe/Ti
1111 molar ratio in samples from the Mount McRae Shale (organic-rich shales) and Brockman Iron
1112 Formation (all other lithologies). Low Fe/Ti molar ratio indicates a predominantly detrital Fe
1113 flux, while high Fe/Ti molar ratio points to a higher flux of authigenic Fe.

1114
1115 **Fig. 4.** Variations in organic C and whole-rock N contents and isotopic compositions, and C
1116 isotope values of whole-rock carbonate as a function of the depth in the drill-core for samples
1117 from the Mount McRae Shale (organic-rich shales) and Brockman Iron Formation (all other
1118 lithologies). Data of Garvin et al. (2009) for the Mount McRae Shale are also plotted for
1119 comparison. See the main text for further discussion. Since samples of Garvin et al. (2009) were
1120 collected from other drill-core (ABDP-9) at a different location in the Hamersley Province
1121 (21°59'29.5"S, 117°25'13.6"E), the depths reported in their paper were adjusted (shifted down by
1122 275 m) in order to obtain a continuous profile of C and N contents and $\delta^{13}\text{C}_{\text{org}}$ and $\delta^{15}\text{N}$ values.

1123
1124 **Fig. 5.** Organic C content versus C isotope composition of carbonates in samples from the Mount
1125 McRae Shale (organic-rich shales) and Brockman Iron Formation (all other lithologies). A
1126 positive trend (albeit with large deviations) suggests that organic matter mineralization was
1127 associated with precipitation of secondary carbonates during diagenesis.

1128
1129 **Fig. 6.** Nitrogen content as a function of organic carbon content (A) and whole-rock potassium
1130 content (B) in samples from the Mount McRae Shale (organic-rich shales) and Brockman Iron
1131 Formation (all other lithologies). (C) C/N molar ratio versus whole-rock potassium content.
1132 Positive correlation in (A) suggests that N was derived from organic matter and in (B) that N was
1133 at least partially in form of NH_4^+ substituting for K^+ in stilpnomelane. Decrease in C/N molar ratio
1134 with increasing K_2O content indicates that NH_4^+ , released from organic matter via mineralization,
1135 was partially trapped in stilpnomelane.

1136
1137 **Fig. 7.** Nitrogen isotope composition versus C_{org}/N molar ratio (A), N concentration (B), and C
1138 isotope values of carbonate (C) in samples from the Mount McRae Shale (organic-rich shales)
1139 and Brockman Iron Formation (all other lithologies). Decoupling among these parameters
1140 suggests that N loss related to diagenesis did not induce any systematic N isotope shift,
1141 supporting preservation of primary $\delta^{15}\text{N}$ values.

1142
1143 **Fig. 8.** Schematic models illustrating N biogeochemical cycle in (A) anoxic water column with
1144 local O_2 production (noted as “oxygen oases”), (B) fully anoxic water column, and (C) redox-
1145 stratified water column. In these models, high productivity is restricted to proximal facies due to
1146 a higher nutrient supply as recorded by organic-rich shales of the Mount McRae Shale, while
1147 lower productivity is typical for distal environments as represented by the Brockman Iron
1148 Formation. High productivity in the Mount McRae Shale depositional environment likely limited
1149 NH_4^+ and NO_3^- availability for biological assimilation, thus inducing larger contribution of N_2 -
1150 fixing bacteria to the biomass resulting in lower $\delta^{15}\text{N}$ values. Co-variation of $\delta^{15}\text{N}$ and $\delta^{13}\text{C}_{\text{carb}}$ values
1151 in the Brockman Iron Formation (Fig. 4) requires a connection between N and Fe biogeochemical
1152 cycles in the water column (see the main text for further details). Under anoxic conditions
1153 (models A and B), the dominant N species available for biological assimilation in the photic zone
1154 would be NH_4^+ . Positive $\delta^{15}\text{N}$ values under these conditions may reflect partial consumption of
1155 NH_4^+ by O_2 -driven nitrification (A) or microbial oxidation utilizing Fe(III) oxyhydroxides (B)
1156 formed in the water column. Under redox-stratified conditions (model C), N in the form of NO_3^-
1157 would be assimilated by primary producers. Highly positive $\delta^{15}\text{N}$ values would be expected under

1158 high denitrification conditions, related to high rates of microbial Fe(II) oxidation at the redox
1159 boundary.

Figure 1

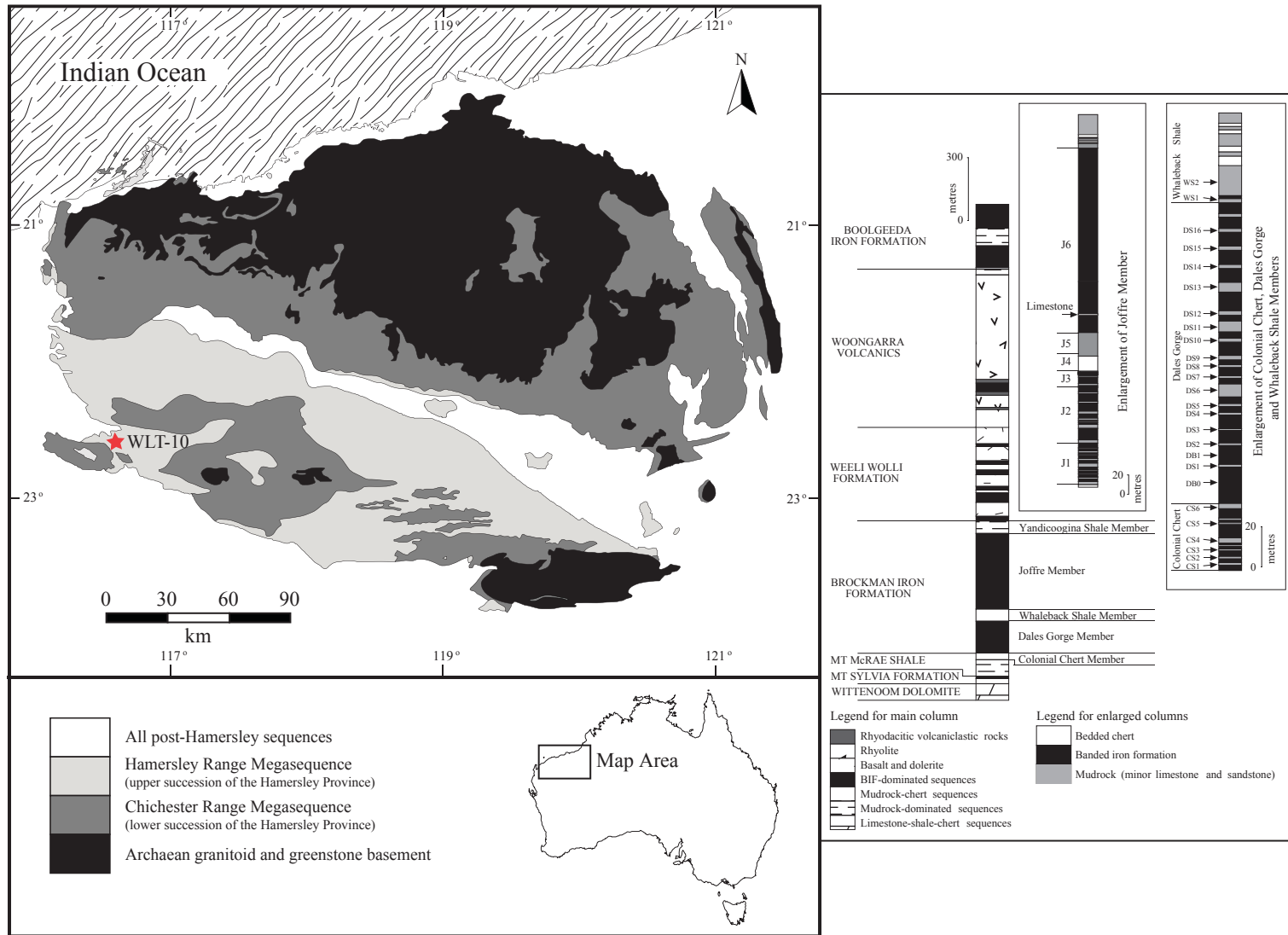


Figure 2

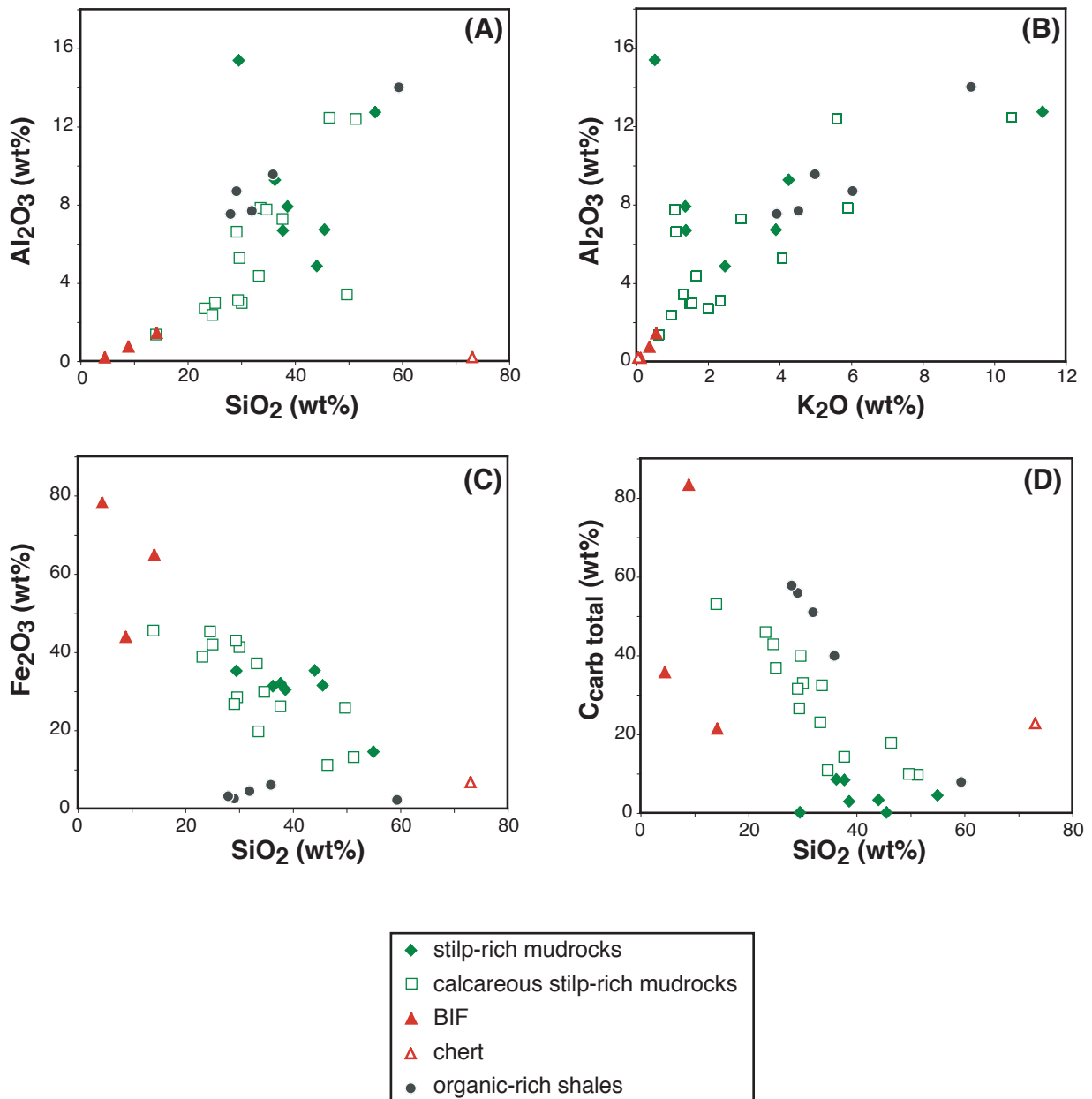


Figure 3

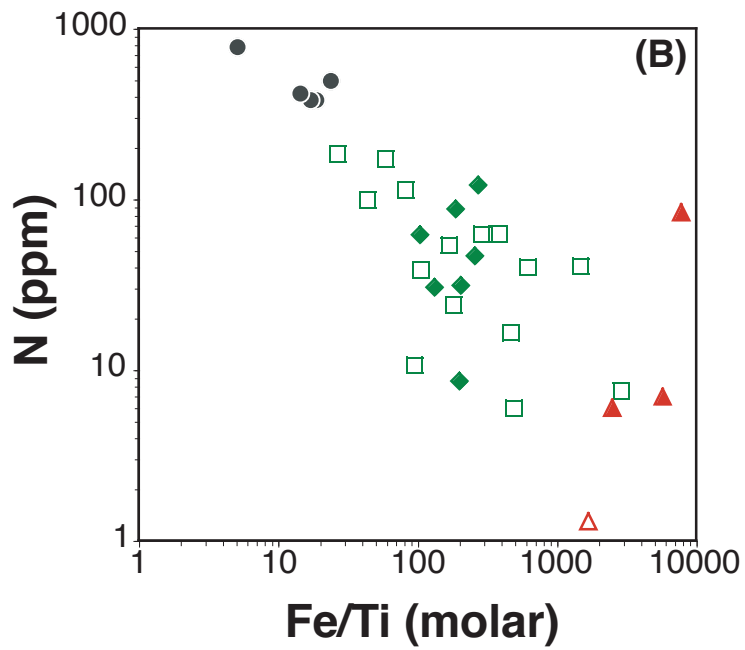
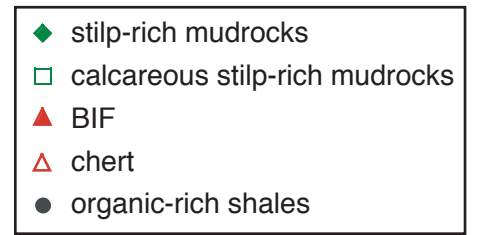
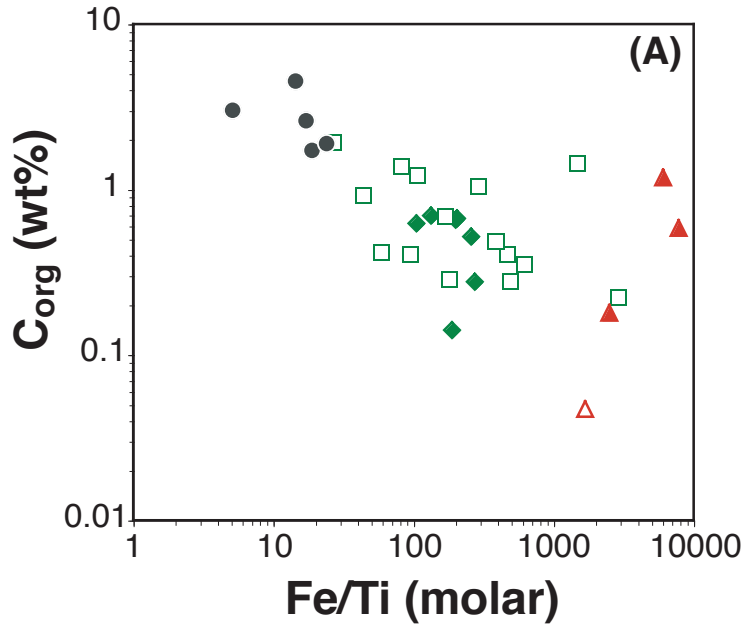


Figure 4

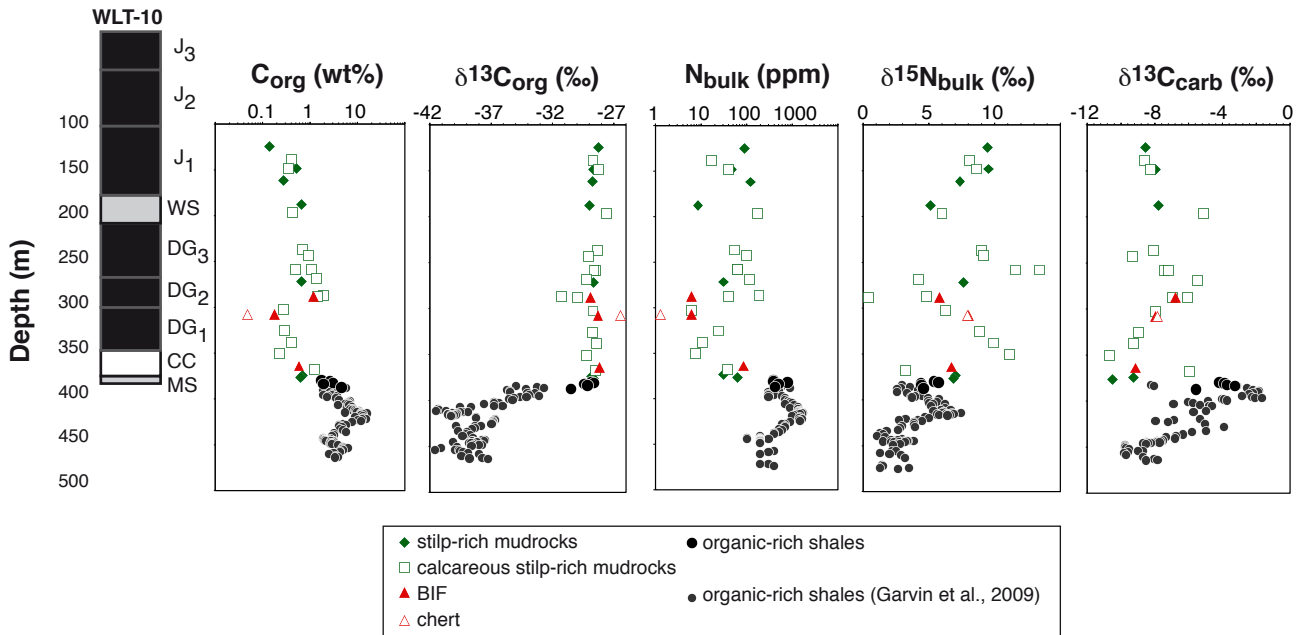
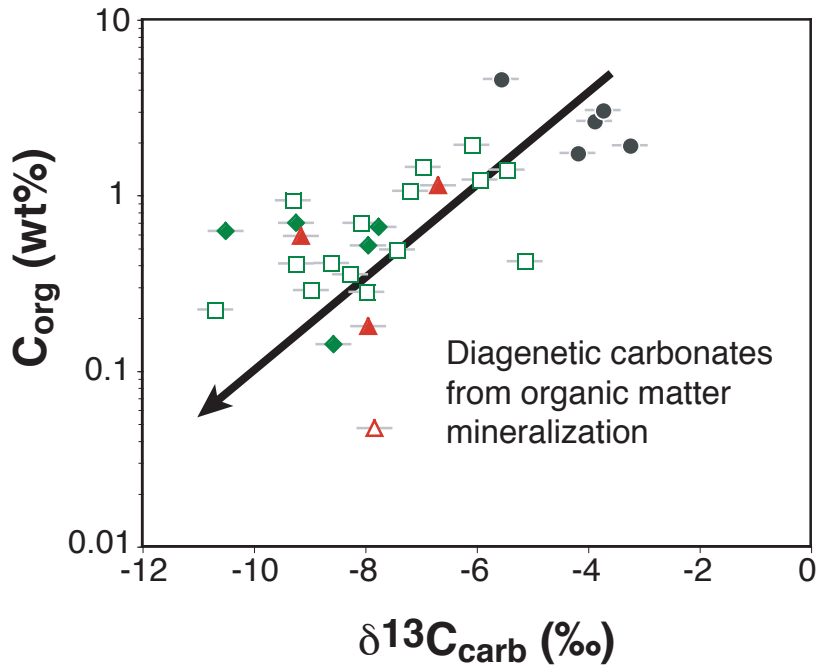


Figure 5



- ◆ stilp-rich mudrocks
- calcareous stilp-rich mudrocks
- ▲ BIF
- △ chert
- organic-rich shales

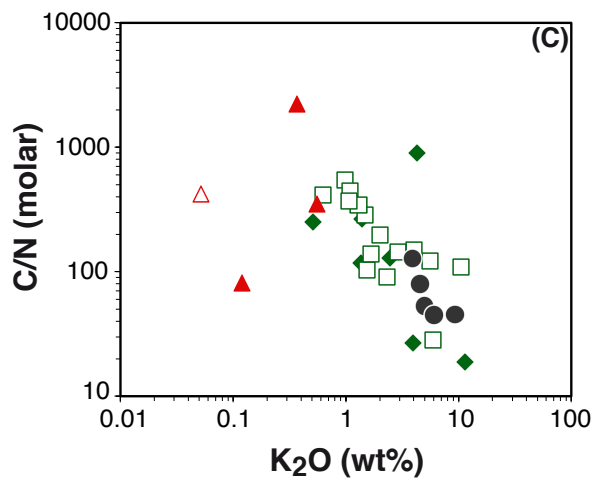
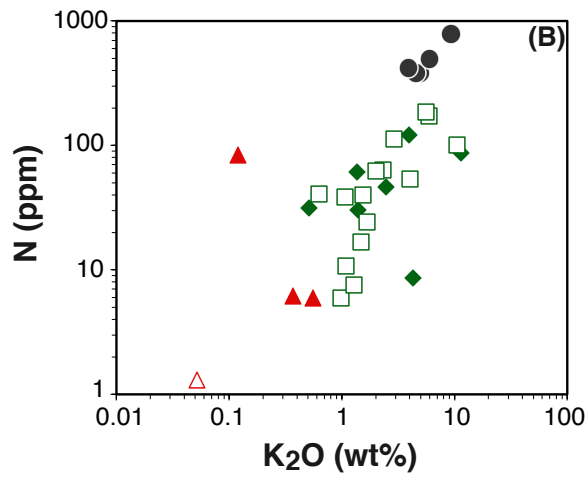
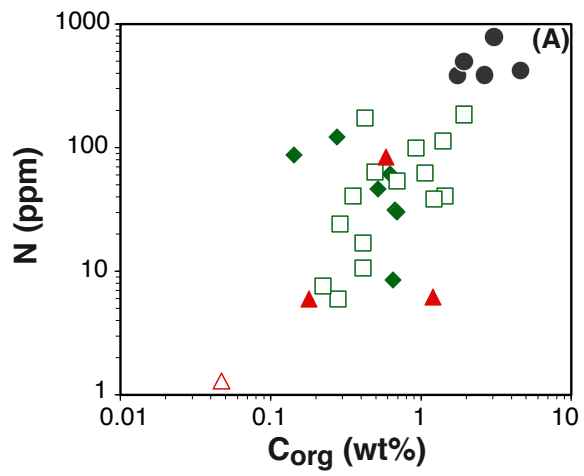


Figure 6

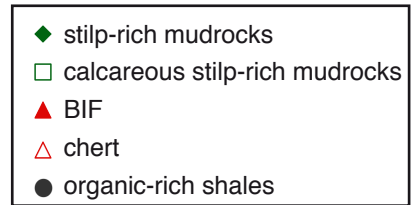


Figure 7

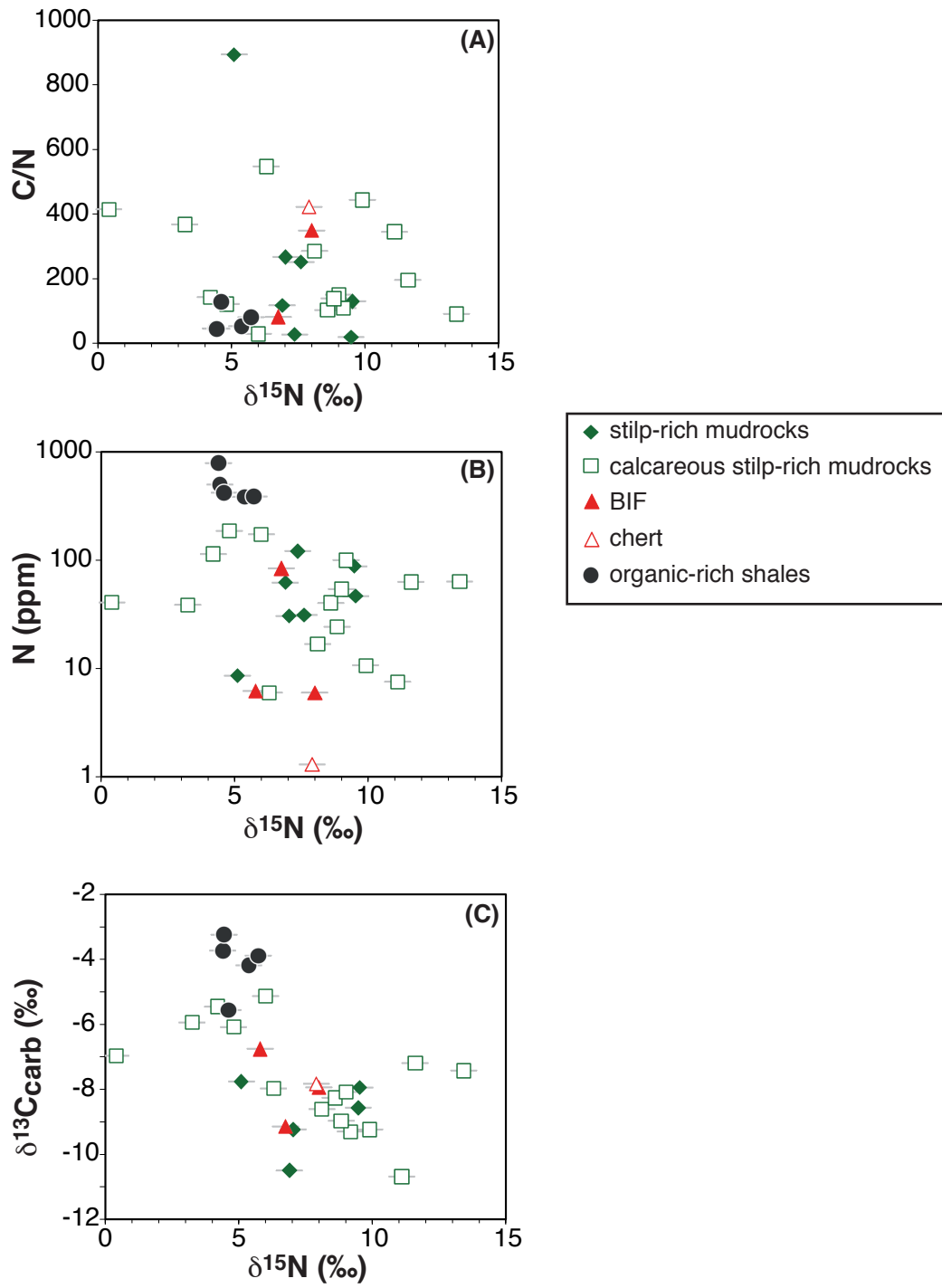
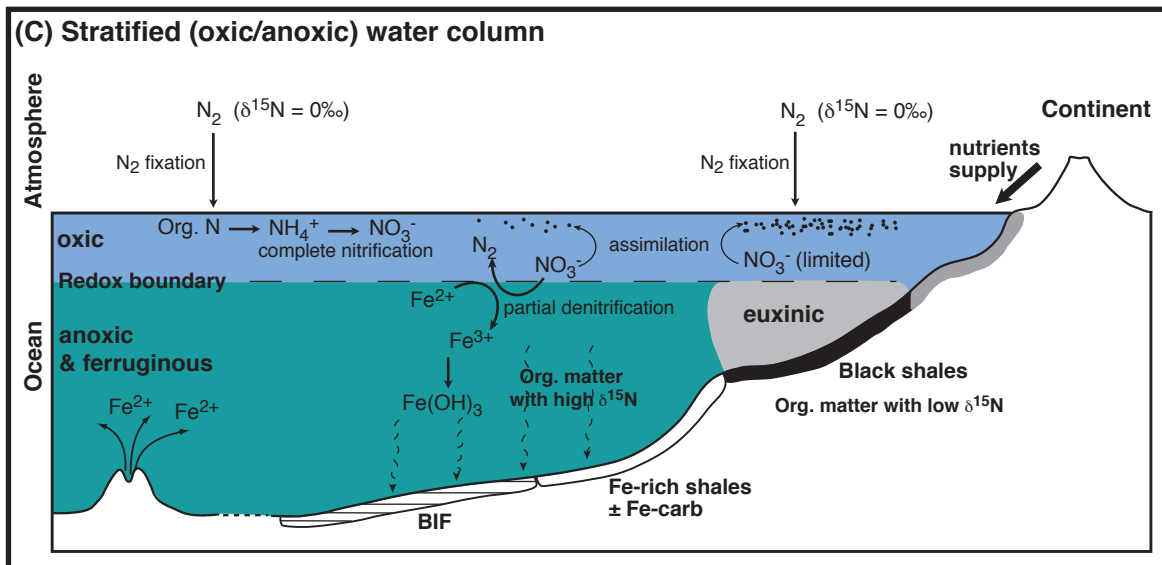
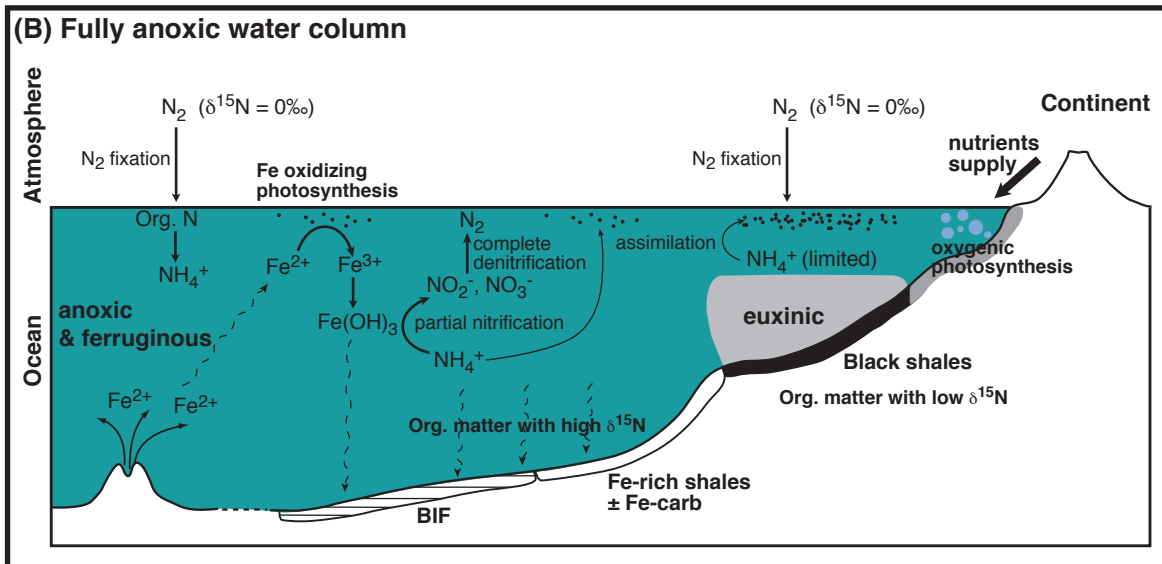
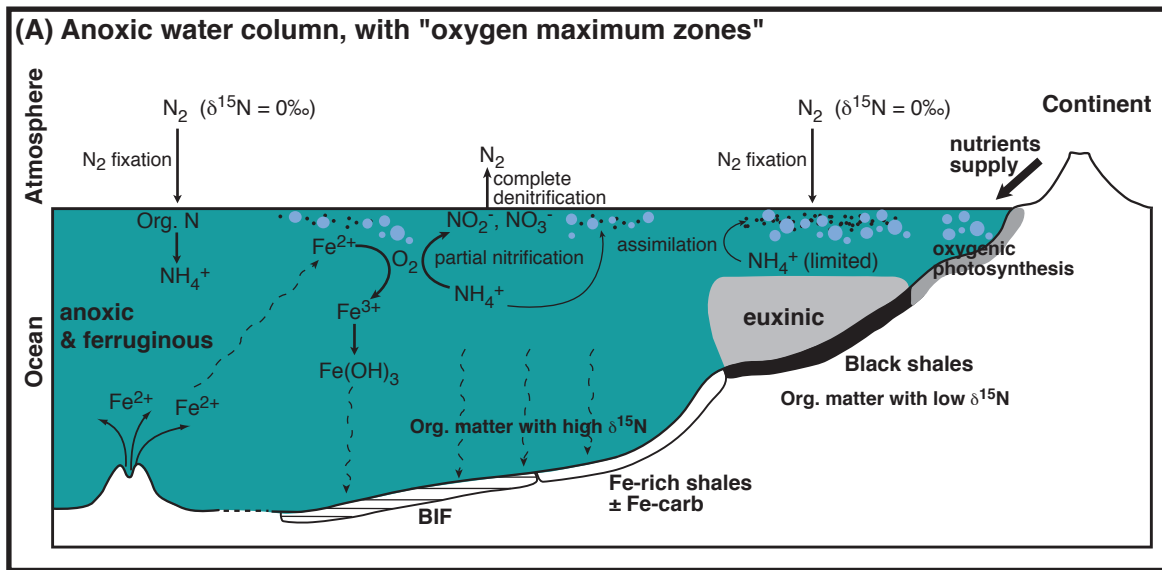


Figure 8



- | | |
|--|--|
| <p>← Brockman Iron Formation →</p> <ul style="list-style-type: none"> - low nutrients - low productivity - high $\delta^{15}N$ | <p>← Mount Mc Rae Shale →</p> <ul style="list-style-type: none"> - high nutrients - high productivity - low $\delta^{15}N$ |
|--|--|